POLITECNICO DI TORINO

Master of Science in Mechanical Engineering

Master's Thesis

Design of a pneumatic back pressure sensor to be integrated into a pneumatic cylinder

Supervisors:

Prof. Luigi Mazza

Prof. Andrea Manuello Bertetto

Candidate:

ALI FAOUR

Contents

Table of Contents

Table of Figures

Table of Tables

Abstract

This thesis presents the design, development, and integration of a pressure sensor for a pneumatic cylinder system, utilizing SolidWorks for 3D modelling, Computational Fluid Dynamics (CFD) simulations for performance analysis, and manufacturing processes for prototyping. The study focuses on designing a robust and efficient pressure sensor capable of accurately monitoring the internal pressure within a pneumatic cylinder. The sensor is designed using SolidWorks, where detailed 3D models are created to ensure optimal functionality and compatibility with the pneumatic system. CFD simulations are then employed to analyse the fluid dynamics within the system, optimizing the sensor design for accuracy and response time under varying operational conditions. Based on the simulation results, the sensor prototype is manufactured, and its performance is evaluated through experimental testing. The sensor's integration into the pneumatic system enhances operational precision and safety by providing real-time pressure monitoring and failure detection. The results demonstrate the sensor's effectiveness in detecting pressure fluctuations and its contribution to the overall reliability of the pneumatic cylinder system. The developed sensor offers a practical solution for improving the performance and longevity of pneumatic systems in industrial applications.

Chapter 1: Introduction and Literature review

Elastomeric seals play an indispensable role in the functionality of pneumatic and hydraulic systems. These systems, widely used across industries such as automotive, aerospace, manufacturing, and construction, depend on elastomeric seals to maintain their efficiency and reliability. The seals are particularly vital in devices featuring reciprocating or oscillating sliding motions, including cylinders, valves, and rotary or semi-rotary motors.

Figure 1: Three-piece radial seal cross-section. Adapted from Parker Hannifin Corporation (n.d.).

The primary purpose of elastomeric seals is to prevent leakage of fluids or gases within the system. This is critical not only for the proper functioning of the equipment but also for ensuring safety and minimizing environmental impact. Elastomeric seals achieve this by forming a tight barrier between two surfaces, which can withstand significant variations in pressure, temperature, and mechanical stress. This sealing capability is crucial for maintaining the efficiency and longevity of pneumatic and hydraulic systems.

In addition to leakage prevention, elastomeric seals are designed to reduce friction between moving parts. By minimizing friction, these seals contribute to the overall energy efficiency of the system and help reduce wear and tear on components. This, in turn, leads to lower maintenance requirements and extended service life for the machinery. The ability to balance sealing performance with low friction is a hallmark of high-quality elastomeric seals.

The materials used for elastomeric seals are equally important in ensuring their effectiveness. These seals are typically made from durable, flexible materials such as nitrile rubber, silicone, or fluorocarbon. The choice of material depends on the specific operating conditions, such as exposure to extreme temperatures, aggressive chemicals, or high-pressure

environments. Advanced manufacturing techniques further enhance the properties of these materials, enabling seals to meet the demanding requirements of modern pneumatic and hydraulic systems.

Moreover, the design of elastomeric seals is tailored to the needs of each application. Factors such as the type of motion, pressure levels, and fluid compatibility are carefully considered during the design process. Innovations in seal design, including the use of advanced geometries and surface treatments, continue to improve the performance and reliability of these components.

In conclusion, elastomeric seals are essential for the optimal performance of pneumatic and hydraulic systems. By preventing leakage, reducing friction, and withstanding challenging operating conditions, these seals ensure the reliability, efficiency, and longevity of the equipment they serve. As industries continue to demand higher performance and sustainability, the role of elastomeric seals remains critical in meeting these evolving challenges.

However, over time, wear and tear during operation can significantly compromise their performance. Factors such as friction, pressure, temperature, and exposure to aggressive fluids contribute to the gradual degradation of seals. This deterioration not only affects their ability to maintain a tight seal but also leads to increased leakage, reduced efficiency, and, in severe cases, system failure. Such issues can disrupt operations, increase energy consumption, and lead to higher maintenance costs, ultimately impacting the reliability and longevity of the system.

Figure 2: Seal, notched. (Stockwell Elastomerics, 2020)

Recognizing the importance of addressing these challenges, researchers and engineers have turned their attention to developing advanced methods for evaluating seal performance and predicting potential failures. A key focus area has been the creation of wear testing methods that provide insights into material loss under various operating conditions. These methods help simulate real-world scenarios, enabling a deeper understanding of how seals respond to stress, friction, and other environmental factors. By analysing the data obtained from wear testing, engineers can identify critical thresholds where seals are likely to fail and implement preventative measures.

Beyond testing, advancements in material science have also played a pivotal role in enhancing seal performance. Researchers are exploring innovative materials with superior resistance to wear, high-temperature stability, and compatibility with a range of chemicals. For instance, the development of composites and elastomers with tailored properties has opened new possibilities for creating seals that can withstand demanding environments. Additionally, coatings and surface treatments designed to reduce friction and minimize wear are becoming increasingly common in modern seal designs.

Moreover, predictive maintenance strategies are being integrated into seal management practices. By employing sensors and monitoring systems, operators can detect early signs of seal wear and take proactive steps to address issues before they escalate. This approach not only reduces downtime but also extends the operational lifespan of seals and improves overall system efficiency.

In conclusion, the challenges posed by wear and tear in seals have driven significant advancements in testing methodologies, material development, and maintenance strategies. These efforts are not only improving the reliability and durability of seals but also enhancing the performance of the systems they serve. As research continues to evolve, the industry is poised to benefit from innovations that ensure greater efficiency, reduced environmental impact, and cost-effective[1]e operations.

Mofidi and Prakash (2008) conducted a study to investigate how counterface surface topography influences the sliding friction and wear behaviour of elastomers under dry sliding conditions. By varying the roughness and texture of counterface materials, the researchers examined their impact on sealing performance and potential failure mechanisms.

Their findings highlighted that counterface surface topography significantly affects the friction and wear behaviour of elastomers. Smoother or optimally textured surfaces were shown to reduce friction and minimize material loss, thereby enhancing sealing performance. Wear patterns observed during the study revealed that surface roughness features, such as peaks and valleys, played a critical role in elastomer deformation and material removal. These results emphasize the importance of surface design in preventing premature seal failure.

However, the study had several limitations. It focused exclusively on dry sliding conditions, which do not account for lubrication commonly encountered in real-world applications. The range of elastomer and counterface materials investigated was narrow, limiting the generalizability of the findings. Additionally, the study did not consider environmental factors such as temperature and humidity or dynamic and variable loading conditions, which are critical in many practical applications. Another limitation was the focus on short-term wear, providing limited insight into long-term sealing performance. Furthermore, the experimental setup required the removal of the seal after each test for examination, which is not representative of in-situ conditions commonly encountered in practical applications.

This study underscores the critical role of counterface surface topography in determining elastomer performance under dry sliding conditions while highlighting the need for further research to address the identified limitations.

In recent years, advancements in wear measurement techniques have significantly contributed to the understanding of seal performance and durability. Among the most notable methodologies is the approach described by Belforte et al. ("Non-Contact Wear Measurement on Pneumatic Seals"), which utilizes laser-based measurement techniques to assess wear in pneumatic seals. This paper introduces a non-contact methodology that leverages a laser displacement sensor integrated into a custom test bench for accelerated life testing. The ability to measure wear without disassembling the seals represents a substantial improvement over traditional techniques that rely on weight or volume loss measurements, which are prone to inaccuracies.

The study highlights several advantages of this approach, such as the precise evaluation of wear patterns and the ability to detect modifications in seal profiles. One critical finding is the non-uniformity of wear across the seal circumference, with initial wear predominantly

occurring in localized regions before progressing toward seal failure. The methodology's application to accelerated life testing enables efficient comparison of different seal prototypes, providing valuable insights for material selection and design optimization.

Despite its merits, the study identifies several limitations. These include the inability to account for environmental factors such as humidity, temperature fluctuations, chemical exposure, and abrasive particles, all of which can influence seal wear in practical applications. Furthermore, the high cost of laser sensors and the specialized equipment required for this method make it less accessible for smaller industries or cost-sensitive projects. Additionally, the technique demands skilled personnel for both operation and maintenance, further constraining its applicability.

Incorporating these findings into the broader context of seal durability studies emphasizes the need for advanced, reliable, and cost-effective wear measurement techniques. Future research could address the identified limitations, potentially enhancing the utility and accessibility of non-contact wear measurement methods across various industrial applications.

The article "A Very High Precision System to Measure Wear in Elastomeric Seals" (IMTC 1996) introduces a cutting-edge methodology and system to assess wear in pneumatic seals with an unprecedented level of precision. The study's primary focus lies in developing an experimental framework capable of providing accurate, real-time measurements of wear progression in elastomeric seals, a critical component in numerous industrial applications. The system leverages a back-pressure sensor to detect subtle pressure variations that correlate directly with seal wear and degradation. Unlike traditional wear assessment techniques that often involve direct contact with the material, this system operates non-invasively, thereby preserving the integrity of the seal during the testing process. This non-contact measurement approach represents a significant advancement in the field, as it eliminates the risk of further

wear or damage introduced by the measurement process itself. Additionally, the use of high-precision sensors enhances the system's sensitivity, enabling it to detect minute changes in backpressure that would otherwise go unnoticed. This capability ensures a high degree of accuracy in quantifying wear, making the system particularly suitable for research and industrial settings where reliability is paramount.

A notable strength of the experimental setup is its ability to maintain a controlled testing environment. By carefully managing environmental factors such as temperature, pressure, and humidity, the researchers ensured consistent and reproducible results. This controlled approach is crucial for isolating the effects of operational conditions on seal wear, allowing for a more comprehensive understanding of the material's performance. The system also features advanced data collection and analysis capabilities, which facilitate real-time monitoring of pressure variations. The data collected is then analysed to evaluate wear progression over time, providing detailed insights into the wear mechanisms of elastomeric seals. This combination of precise measurement and robust data analysis underscores the system's utility in advancing our understanding of seal wear.

The findings of the study highlight the system's effectiveness in detecting wear with remarkable precision. The researchers demonstrated that even small variations in backpressure could be accurately measured and directly correlated to the wear of the seal. This high sensitivity not only validates the system's reliability but also opens new avenues for investigating the subtle nuances of seal degradation. Additionally, the study revealed distinct wear patterns that emerged over repeated operational cycles. These patterns, characterized by specific changes in pressure, provide valuable insights into the wear behaviour of elastomeric materials under varying conditions. By identifying these patterns, the research contributes to a

deeper understanding of the underlying mechanisms that govern seal wear, which is critical for improving the design and performance of these components.

From a practical standpoint, the method and system presented in the study hold significant potential for industrial applications. Pneumatic seals play a vital role in ensuring the proper functioning of actuators, valves, and other machinery. Their reliability and longevity are crucial for maintaining operational efficiency and minimizing downtime. The ability of this system to provide detailed and accurate wear assessments makes it an invaluable tool for industries that depend on the performance of elastomeric seals. Furthermore, the insights gained from these assessments can inform the development of more durable seal materials and designs. By understanding how seals degrade under typical operating conditions, engineers can optimize material properties and geometries to enhance durability and performance.

In conclusion, the article "A Very High Precision System to Measure Wear in Elastomeric Seals" presents a novel and highly effective approach to assessing wear in pneumatic seals. By a non-contact back-pressure sensor, high-precision measurement capabilities, and a controlled experimental environment, the system provides unprecedented insights into the wear mechanisms of elastomeric materials. The findings of the study have far-reaching implications for both research and industry, offering a valuable tool for improving seal reliability and guiding the development of advanced seal designs. As industries continue to demand higher levels of performance and durability from their components, the methodologies outlined in this research represent a significant step forward in meeting these challenges.

Non-contact distance measurement is a critical requirement in automated machinery and inspection systems, particularly in applications requiring high precision. Traditional sensors in the 0 to 200 μm range are often prohibitively expensive, while low-cost alternatives,

such as air-jet sensors, have been explored for narrower ranges. Belforte, Manuello Bertetto, and Raparelli (1995) presented a non-contact pneumatic sensor designed for high-precision distance measurement in the 0 to 200 μm range, offering both high reliability and low cost.

The sensor is based on a flapper-nozzle system, consisting of a pressure source, a fixed resistance, a measuring chamber, and an exhaust nozzle. The use of compressed air as the sensing medium makes it suitable for harsh environments, such as high-temperature or contaminated areas, where traditional sensors might fail. Additionally, the low cost and high reliability of this sensor make it an attractive option for integration into automated inspection systems and processing equipment

A theoretical model was developed to study the sensor's static and dynamic behaviour, addressing limitations in existing models. The proposed model accounts for the nonlinearities of fluid resistances and the continuous phenomena during exhaust nozzle closing. Experimental validation showed that the sensor performs reliably in both static and dynamic conditions, with results closely matching theoretical predictions.

Despite its advantages, the sensor has several limitations. It is designed for a relatively narrow range of 0 to 200 μm, which may not be sufficient for applications requiring larger measurement ranges. Additionally, its performance could be affected by environmental factors such as temperature fluctuations and air contamination. The complexity of the theoretical model may also pose challenges for implementation. Future research could explore extended measurement ranges, improved environmental robustness, and simplified implementation methods.

In our research, we focus on detecting and predicting seal failure specifically in the pneumatic head of a pneumatic cylinder, a critical area that is highly susceptible to failure under high loads. To achieve this, we propose the integration of a distance sensor within the sealing

zone, more specifically a Back Pressure Sensor. This sensor will continuously monitor displacement during high-load conditions, capturing real-time data that reflects the seal's behaviour. By analysing these displacements, we can establish a correlation between abnormal behaviour and impending seal failure.

To better understand the system's functionality, we utilized flow simulation in SolidWorks to analyse its performance under various conditions. Based on these insights, we suggest using 3D printing to manufacture the product, enabling precise customization and rapid prototyping.

Additionally, our approach includes utilizing advanced algorithms to process the sensor data, enabling accurate predictions of failure timelines. By identifying early signs of wear or failure, this system allows for timely interventions, preventing catastrophic failures and reducing downtime. Moreover, the integration of such monitoring systems offers a dual benefit: enhancing the reliability of pneumatic systems and providing valuable insights into the relationship between operational conditions, seal wear, and failure mechanisms. This proactive detection method paves the way for smarter, more efficient maintenance strategies and longer system lifespans.

Back-pressure sensors function analogously to an electrical circuit with a variable resistor that adjusts output voltage. In fluidic systems, the principle involves manipulating airflow resistance to produce measurable pressure changes. When an object is placed near the sensor's mouth, it disrupts the airflow, increasing resistance and causing a pressure rise at the output port. If the output port is completely closed, the resulting pressure matches the supply pressure.

Unlike electrical systems where the relationship between resistance and output is linear, fluidic sensors exhibit a nonlinear relationship between output pressure and flow rate. This nonlinearity is a fundamental characteristic of fluidic systems, as highlighted by Jacobs (1972). It enables back-pressure sensors to be highly sensitive to variations in proximity or obstruction, making them valuable for applications requiring precise pressure detection.

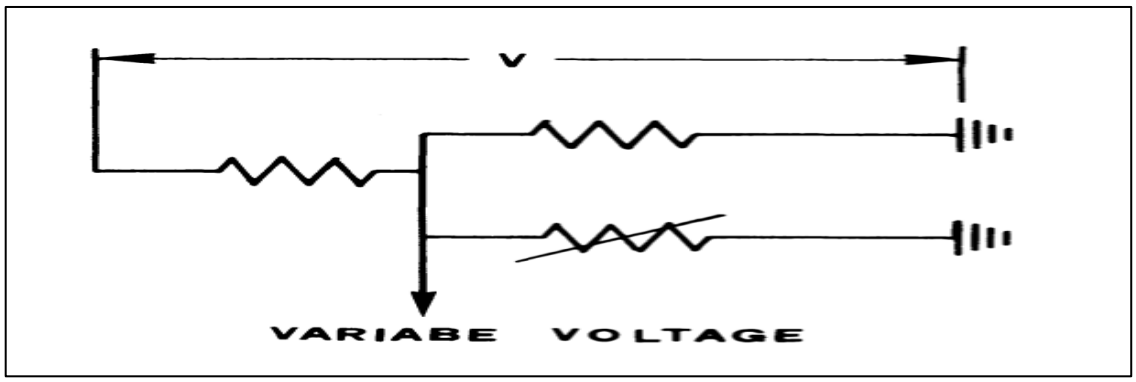

Figure 3: Figure 3: Analogy of back-pressure sensor with an electrical circuit. Reprinted from Fluidic Sensors and Some Large-Scale Devices (p. 8), by B. E. A. Jacobs, 1972, Springer-Verlag Wien-New York. Copyright 1972 by Springer-Verlag Wien.

Chapter 2: Distance Sensor Types, Differences, and Cost

Distance sensors play a crucial role in a wide range of applications, including robotics, industrial automation, consumer electronics, and automotive systems. These sensors allow devices to detect objects and measure distances without physical contact. Various types of distance sensors exist, each based on different operating principles, offering distinct advantages, limitations, and cost considerations.

2.1.1 Ultrasonic Distance Sensors

Ultrasonic sensors determine distance by emitting high-frequency sound waves and measuring the time taken for the reflected echo to return after striking an object. Typically, the sensor includes a transmitter to generate the sound waves and a receiver to detect the returning signal (SensComp, 2021).

Advantages:

Ultrasonic sensors are cost-effective and widely available. They are not affected by the color or transparency of the target object and can reliably measure distances to objects with irregular shapes.

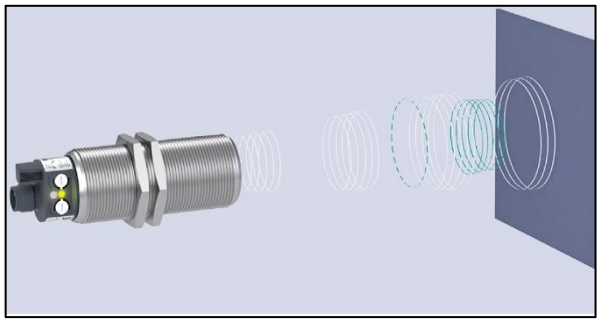

Figure 4: Ultrasonic Sensor Detection Range Comparison Diagram (Pepperl+Fuchs)

Limitations:

Their performance can be influenced by environmental conditions such as temperature, humidity, and air currents (Honeywell, 2022). Additionally, they are less effective when measuring soft or angled surfaces that may absorb or deflect sound waves.

Typical Cost:

Ultrasonic sensors are generally inexpensive, with typical prices ranging from $10 to $50.

2.1.2 Infrared (IR) Proximity Sensors

Infrared sensors work by emitting infrared light and measuring the amount of reflected light from nearby objects to detect their presence and estimate distance. They are commonly used in short-range applications (Sharp Electronics, 2023).

*Figure 5: Figure 5: Circuits-Elec. (n.d.). *Infrared proximity sensor module with 5-36V input*

Advantages:

Infrared sensors offer fast response times and are compact, making them easy to integrate into a wide range of devices. They also consume very little power, which is beneficial for battery-operated applications.

Limitations:

Their performance can be affected by ambient light conditions (Adafruit, 2023) and they are less effective when detecting dark or highly reflective surfaces. Additionally, IR sensors are generally limited to short-range measurements, typically within a few centimeters.

TypicalCost:

IR sensors are highly affordable, with prices usually ranging from $5 to $20.

2.1.3 Laser Distance Sensors

Laser sensors operate using a Time-of-Flight (ToF) principle, where a laser beam is emitted and the time taken for the reflected light to return is measured. This technology provides high precision and is well-suited for long-range distance measurements (SICK, 2023).

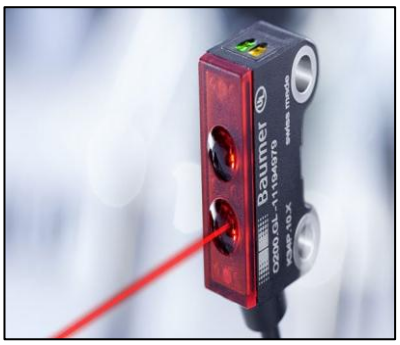

Figure 6: Figure 6: Baumer. (n.d.). O200 miniature laser sensor for precision detection

Advantages:

Laser distance sensors provide high accuracy and fine resolution, making them ideal for applications that require precise measurements. They are capable of long-range detection, often reaching several hundred meters, and their performance remains stable under varying ambient light conditions.

Limitations:

One key drawback is their higher cost compared to ultrasonic and infrared sensors. Additionally, their performance can be affected by environmental factors such as rain, fog, or dust, which may interfere with the laser signal (Leica, 2022).

Typical Cost:

Laser distance sensors are more expensive, with prices ranging from $100 to several thousand dollars.

2.1.4 Capacitive Proximity Sensors

Capacitive sensors detect changes in capacitance caused by the presence of an object. They can sense both conductive and non-conductive materials.

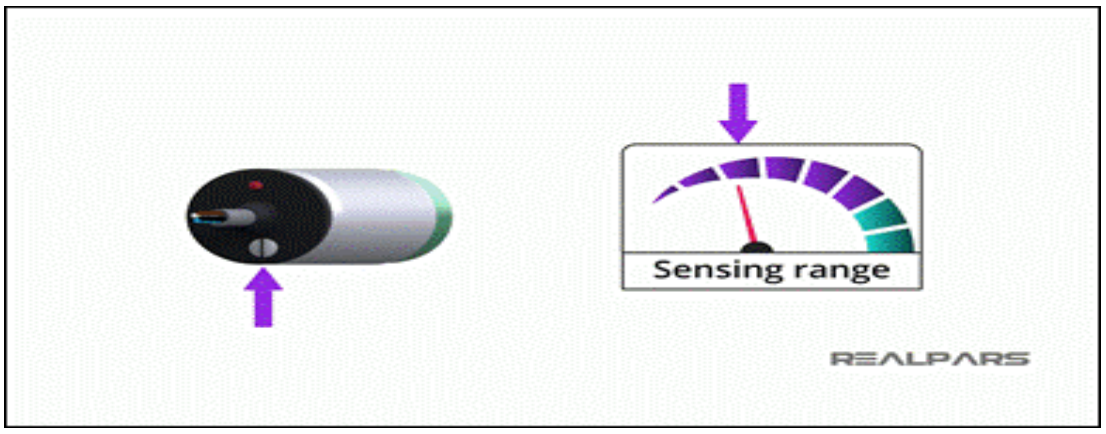

Figure 7: Capacitive Sensor Adjustment Mechanism Showing Sensing Range Modification. Note. From Capacitive Sensors Explained by RealPars, 2024 (https://www.realpars.com/blog/capacitive-sensor). Copyright 2024 by RealPa

Advantages:

Capacitive sensors can detect a wide variety of materials, including liquids, powders, and granular substances (Omron, 2021). They are unaffected by the color or surface reflectivity of the target and can even detect objects through non-metallic barriers, such as glass or plastic.

Limitations:

Their main limitation is the short sensing range, typically restricted to a few centimeters. Additionally, their performance can be influenced by environmental factors such as humidity and temperature variations.

TypicalCost

Capacitive sensors are moderately priced, with typical costs ranging from $20 to $100.

2.1.5 Inductive Proximity Sensors

Inductive sensors generate an electromagnetic field and detect changes caused by the presence of metallic objects.

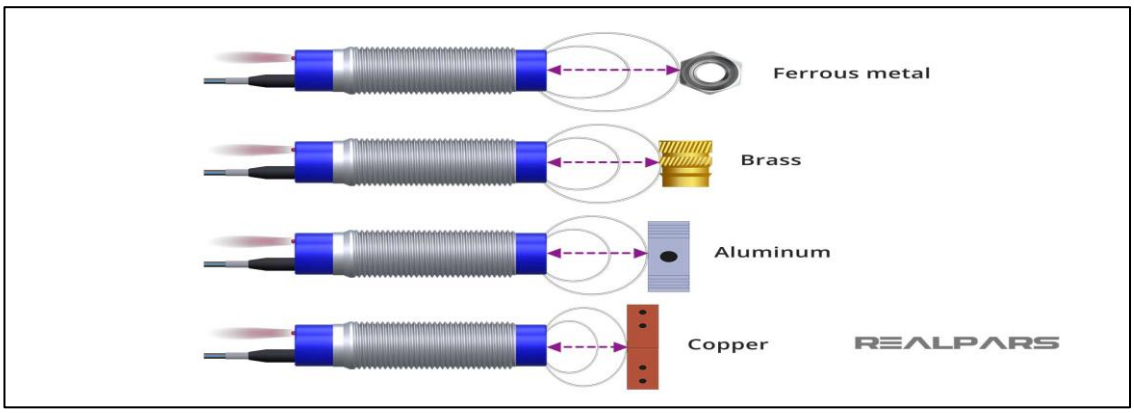

Figure 8: Inductive Sensor Sensing Range Comparison for Different Materials (Ferrous Metal, Brass, Aluminum, and Copper).
Note. From Inductive Proximity Sensors: The Complete Guide by RealPars, 2024 (https://www.realpars.com/blog/inductive-sensor). Copyright 2024 by RealPars.

Advantages:

Inductive sensors are highly reliable when it comes to detecting metal objects and are not affected by non-metallic contaminants such as dust, dirt, or moisture (Schneider Electric, 2023). They are also known for their robustness and durability, making them well-suited for use in harsh industrial environments.

Limitations:

A key limitation of inductive sensors is that they can only detect metallic objects and are ineffective with non-metallic materials. Additionally, their sensing range is relatively limited, typically extending only a few centimeters.

Cost:

Inductive sensors are generally affordable, with prices typically ranging from $10 to $50.

2.2 Fluidic Sensors

2.2.1. Back-Pressure Sensor

A back-pressure sensor works by taking advantage of the pressure changes that occur when a fluid flows through a narrow passage or nozzle. As an object moves closer to the nozzle's opening, it disrupts the airflow, which causes the pressure at the back of the nozzle to

rise. This increase in pressure is then used as a signal to detect the presence of the object (Mech Poriyaan, n.d.).

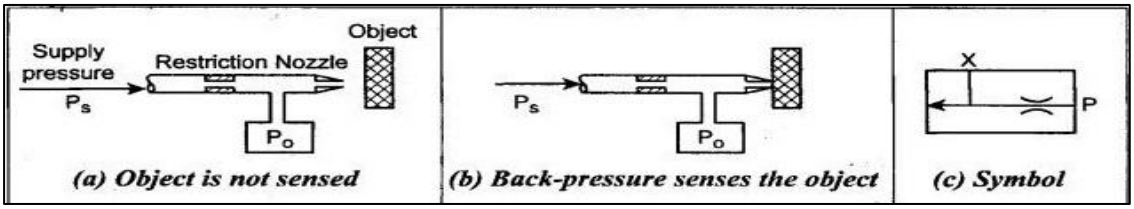

*Figure **9**: Operational States of a Back-Pressure Sensor Showing (a) Idle State with Supply Pressure (P_s) and Restriction Nozzle, (b) Object Detection via Back-Pressure Change (P_o), and (c) Standard Schematic Symbol. Adapted from *Fluid Sensors* by Poriyaan.mech, n.d. (https://mech.poriyaan.in/). Copyright [Year] by Poriyaan.mech.*

- **Working-Principle:**

  In back-pressure sensing, a fluid stream flows continuously through a nozzle. When an object approaches the nozzle's exit, it partially blocks the flow, leading to an increase in back pressure. This change in pressure is detected by the sensor and used to indicate the presence of the object.

- **Applications:**

  Back-pressure sensors are commonly used in industrial automation for detecting small parts and in non-contact sensing applications where handling fragile materials without physical contact is essential.

2.2.2 Cone-Jet Proximity Sensor

The cone-jet proximity sensor features an annular nozzle positioned around a central sensing hole. As fluid exits the nozzle, it forms a conical jet, which creates a low-pressure zone in front of the sensor. When an object moves close to this conical flow, some of the fluid is

reflected back into the low-pressure area, causing an increase in output pressure. This pressure change is then used to signal the presence of the object (Mech Poriyaan, n.d.).

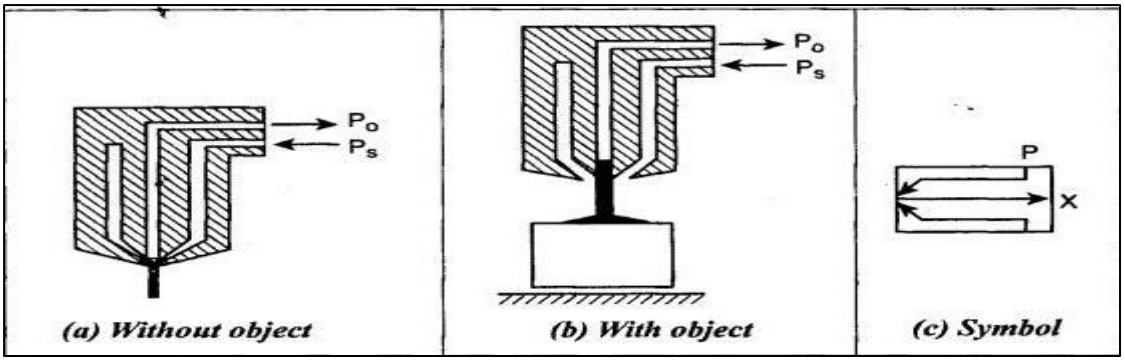

Figure 10: Cone-Jet Proximity Sensor States Showing (a) Default Configuration Without Object, (b) Detection With Object Present, and (c) Standard Industrial Symbol.
Note. Adapted from Fluid Sensors by Poriyaan.mech, n.d. (https://mech.poriyaan.in/). Copyright [Year] by Poriyaan.mech.

- **Working-Principle**

  In this sensor, fluid exits through an annular nozzle in the form of a conical jet. When an object approaches and disrupts this flow, the pressure at the central sensing hole rises. This change in pressure is detected and used to identify the presence of the object.

- **Applications**

  Cone-jet proximity sensors are commonly used in automated assembly lines to detect the presence of components. They are also applied in precision measurement systems where non-contact detection is required.

2.2.3 Interruptible-Jet Sensor (Gap Sensor)

This type of sensor operates by transmitting a continuous air stream from a nozzle across a small gap to a receiver. When an object enters the gap and blocks the air jet, the flow

is interrupted, causing the signal at the receiver to disappear. This change is used to indicate the presence of an obstruction (Mech Poriyaan, n.d.).

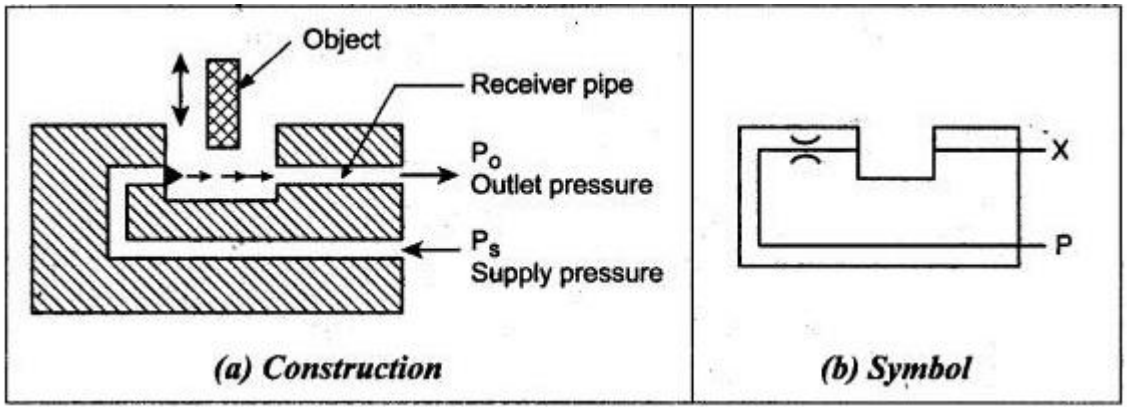

Figure 11: Interruptible Jet Sensor Showing (a) Construction with Key Components (Receiver Pipe, Supply Pressure P_s, Outlet Pressure P_o) and (b) Standard Industrial Symbol. Note. Adapted from Fluid Sensors by Poriyaan.mech, n.d. (https://mech.poriyaan.in/). Copyright [Year] by Poriyaan.mech.

- **Working Principle:**

A continuous air stream is directed from a nozzle across a gap to a receiver. When an object moves into the gap, the air stream is interrupted, and the receiver no longer detects the signal. This absence of the signal indicates the presence of an obstruction.

- **Applications**

Air jet interruption sensors are commonly used in conveyor belt systems to detect the presence or passage of products. They are also applied in automated quality control systems where non-contact detection is required.

Conclusion:

Fluid sensors play a vital role in modern industrial systems by enabling accurate monitoring and control of fluid-related parameters. Different types of sensors—such as back-pressure sensors, cone-jet proximity sensors, gap sensors, are designed to meet specific functional needs. Their widespread use in automation, manufacturing, and safety applications highlights their significance in the field of mechanical engineering. Careful selection of the appropriate sensor based on the system's requirements is essential to ensure optimal performance, reliability, and efficiency (Mech Poriyaan, n.d.).

Chapter 3: Methodology Design and Development of the Back-Pressure Sensor

3.1 Introduction to the Design Process

The back-pressure sensor was designed using SolidWorks (CAD) software that allows modeling, simulation, and optimization of mechanical components. The design process followed a structured methodology consisting of several key stages: concept development, 3D modeling, material selection, structural analysis, and performance evaluation. Each stage played a vital role in ensuring that the sensor met its functional requirements while maintaining durability, reliability, and compatibility with the intended application.

3.2 Concept Development and Design Requirements

The first step in designing the back-pressure sensor was to define clear design requirements based on the specific needs of the application. The sensor needed to accurately measure pressure variations within the system, which required incorporating several key features:

- High sensitivity to detect even small pressure changes
- Robust construction to withstand operating conditions
- Compatibility with the existing system for smooth integration
- A compact and lightweight design for easy installation

To support this process, brainstorming sessions and literature reviews were carried out to gather information on existing sensor designs, industry best practices, and relevant standards. The knowledge gained from this research informed the development of initial sketches and conceptual layouts, which provided the foundation for the 3D modeling phase in SolidWorks.

3.3 Modelling in SolidWorks

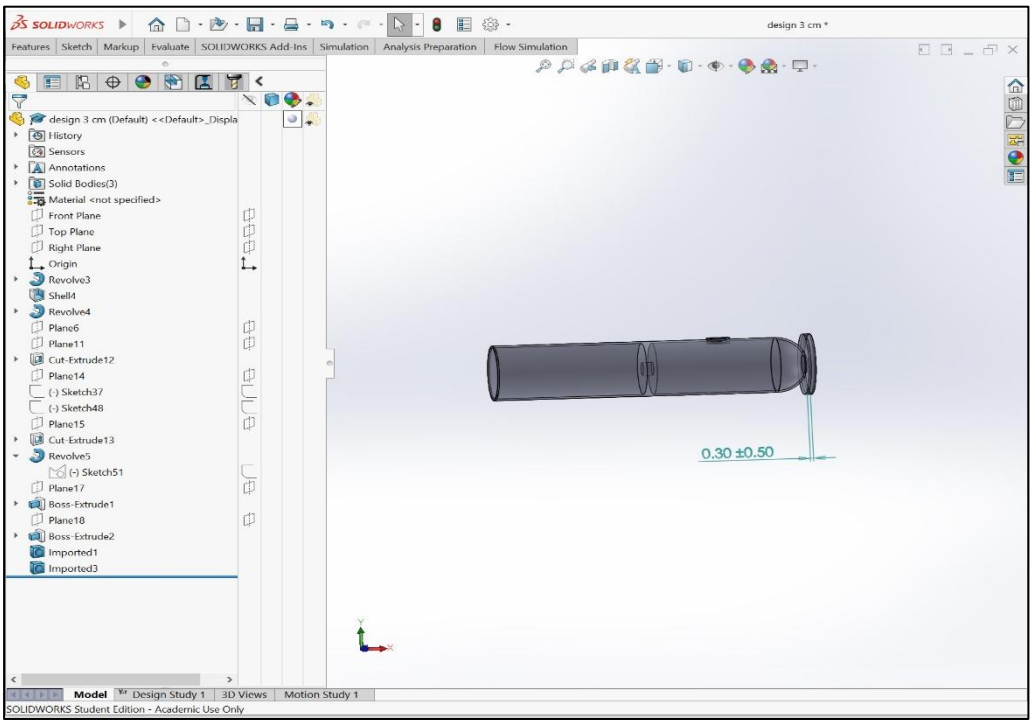

Figure 12: Designed Sensor

Once the design concept was finalized, a detailed 3D model of the back-pressure sensor was developed using SolidWorks. The modeling process involved several key steps:

- **Sketching and Dimensioning:** 2D sketches were created based on engineering calculations, ensuring accurate dimensions and proportions.
- **Feature-Based Modeling:** SolidWorks tools such as extrusions, cuts, fillets, and chamfers were applied to shape the sensor and define its functional features.

3.4 Finite Element Analysis (FEA) and Design Optimization

To evaluate the structural and functional performance of the back-pressure sensor, Finite Element Analysis (FEA) was carried out in SolidWorks. The simulation focused on stress distribution, deformation, and identifying potential failure points under various operating conditions. This analysis guided the optimization of the design through several key actions:

- **Material Reduction:** Unnecessary material was removed to minimize weight while maintaining the sensor's structural integrity.
- **Stress Reinforcement:** Areas prone to stress concentration were reinforced to improve durability and prevent mechanical failure.
- **Manufacturability:** Complex geometries were simplified where possible to ensure the design could be manufactured efficiently.

One of the primary objectives of the simulation was to study the airflow behavior within the sensor, specifically the relationship between airflow and the distance from the sensor's inlet to its outlet. By analyzing velocity and pressure variations along this path, critical insights were gained, such as identifying regions of high resistance, flow recirculation, and potential separation zones. These findings were essential for optimizing the design to reduce energy losses and ensure accurate sensor readings.

The simulation also allowed for a direct comparison between different design iterations. By modifying specific features—such as the inlet shape, internal flow paths, and outlet positioning—we were able to assess their impact on airflow distribution and overall performance. This iterative approach ensured the selection of the most efficient and practical design configuration.

The insights gained through simulation served as a solid foundation for further development. By combining these findings with experimental validation, the design was refined to enhance real-world performance. Ultimately, this process led to a deeper understanding of airflow dynamics within the sensor, contributing to greater accuracy, reliability, and efficiency in its operation.

3.5 Finite Element Modelling

3.5.1 Defining Lids:

Adding lids is an important step to clearly define the fluid domain. A lid is placed at the inlet to control how the fluid enters the system, and another is positioned at the outlet to manage how the fluid exits. These lids help seal the model, creating proper boundaries that are essential for accurate simulation results. By setting these boundaries correctly, the software can better analyse how the fluid behaves inside the system, leading to more reliable outcomes.

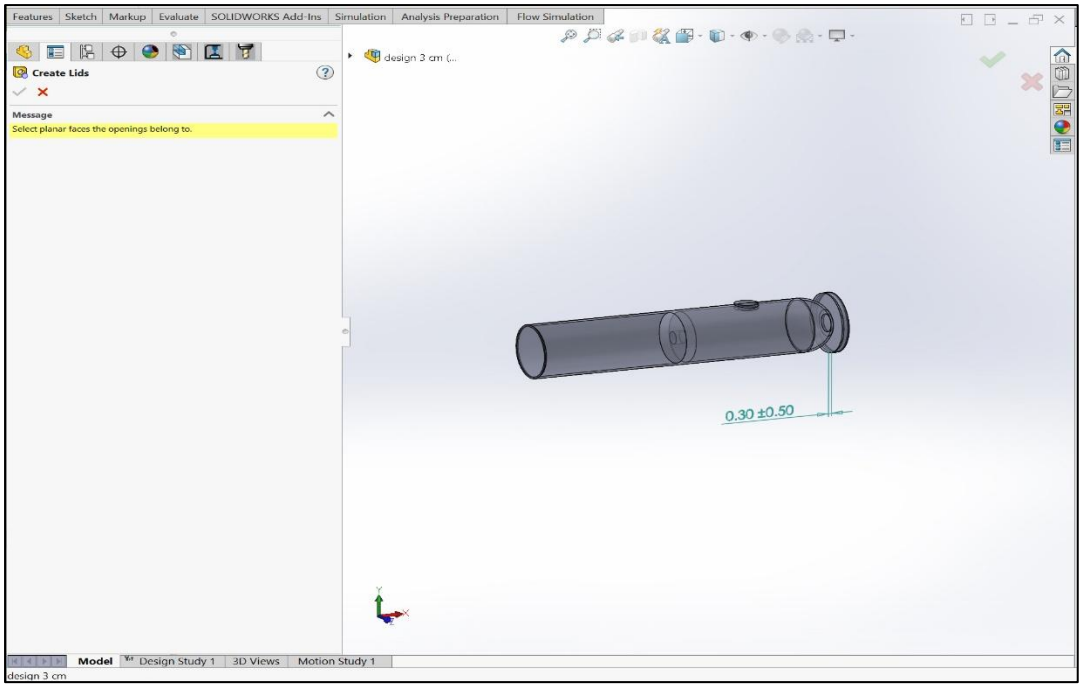

Figure 12:Define Lids

3.5.2 Defining Fluid:

Defining the working fluid is a next step in setting up the analysis. The user selects the appropriate fluid, such as air, from the engineering database to ensure accurate simulation of

real-world conditions. This selection influences key parameters like density, viscosity, and flow behaviour, effect the overall results of the simulation.

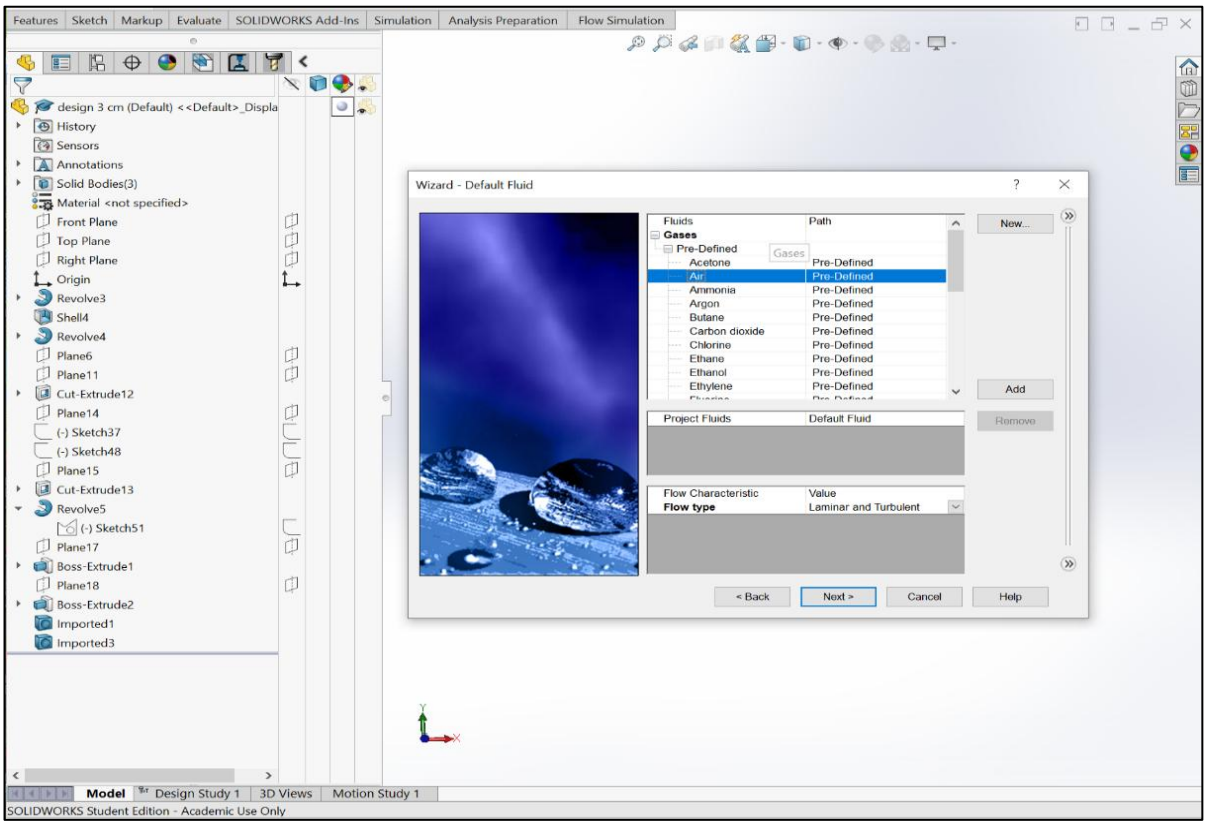

Figure 14:Defining Fluid

2.5.3 Defining Mesh:

Automatic mesh was utilized to balance accuracy and computation time. This automated approach generated a refined mesh where needed while keeping the overall element count manageable. As a result, the airflow behavior through the sensor was analyzed efficiently without requiring extensive manual adjustments. Additionally, this method minimized computational resource usage while still ensuring reliable and meaningful simulation results.

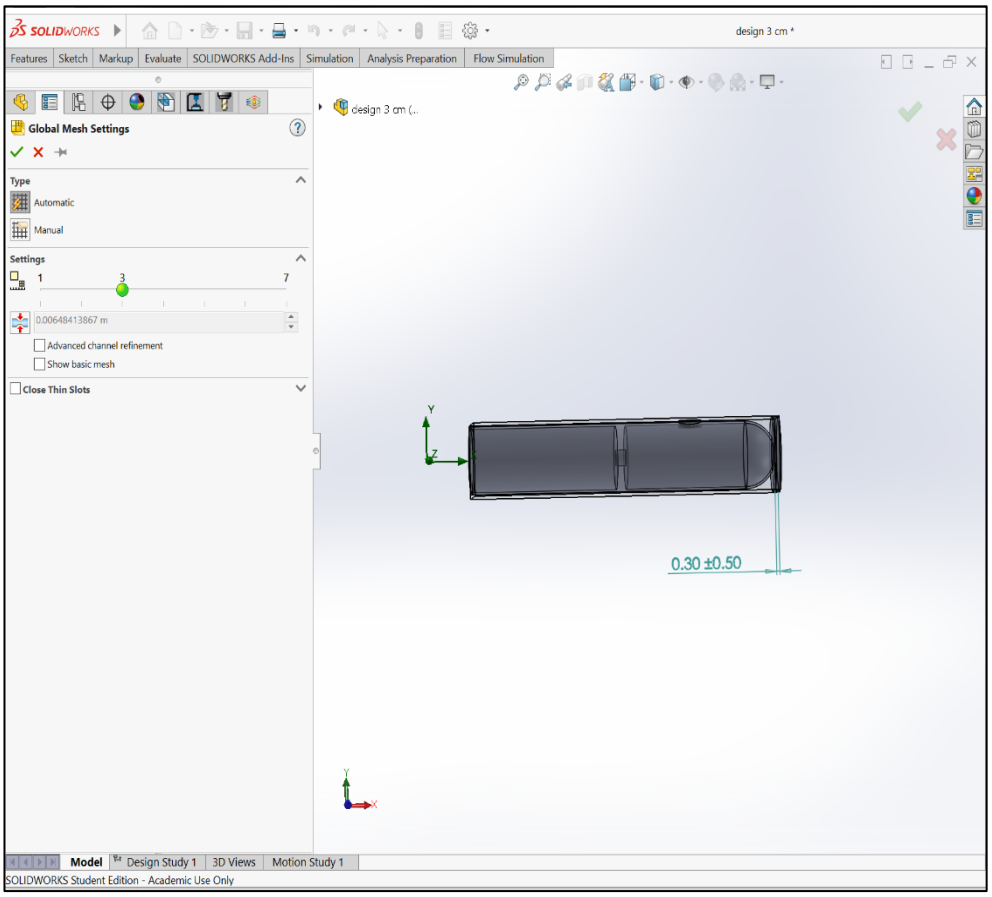

Figure 15: Define Mesh

3.5.4 Defining Boundary Condition at the inlet:

The boundary conditions at the inlet were defined by setting the total pressure to control the airflow entering the system. Four different pressure values—2 bar, 3 bar, 4 bar, and 5 bar—were applied to assess the sensor's response under varying conditions. This approach allowed for a comprehensive evaluation of the sensor's performance across a range of operating pressures. By analyzing multiple pressure scenarios, the simulation provided insights into how the sensor behaves under different airflow conditions, ensuring accurate performance predictions.

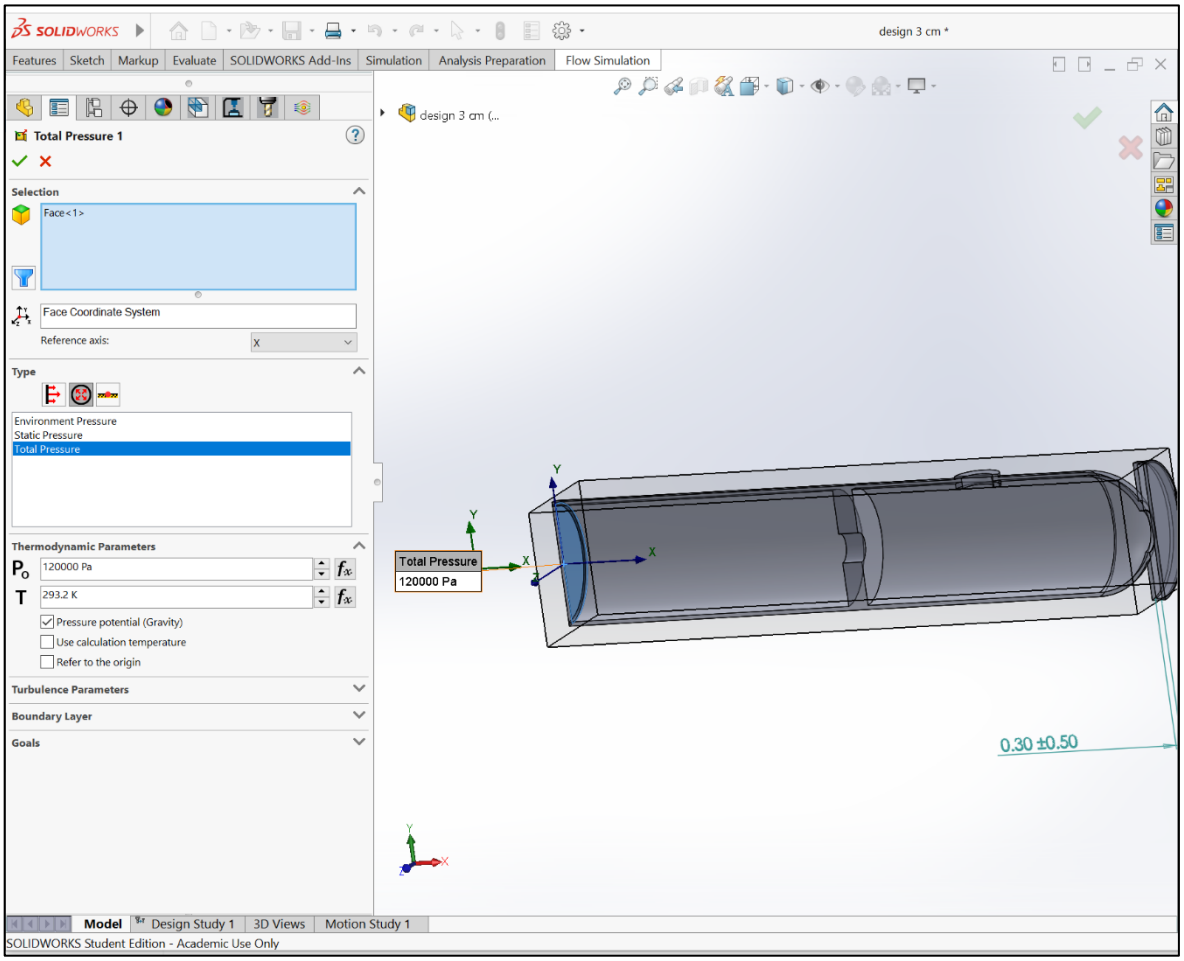

Figure 16: Defining Boundary Conditions at the inlet

3.5.5 Defining Boundary Condition at the Outlet:

Setting the pressure at the outlet to the same level as the surrounding pressure defined boundary conditions. This made the fluid flow out of the system in a way that was like how it would happen in nature. This method helps recreate the real-world conditions in which the fluid interacts with the things around it. Setting the outlet pressure to the same level as the surrounding air makes the simulation more like how the system would work in real life. This boundary condition makes sure that the flow is released correctly without changing the pressure at the outlet in a way that isn't natural, which gives the analysis reliable results.

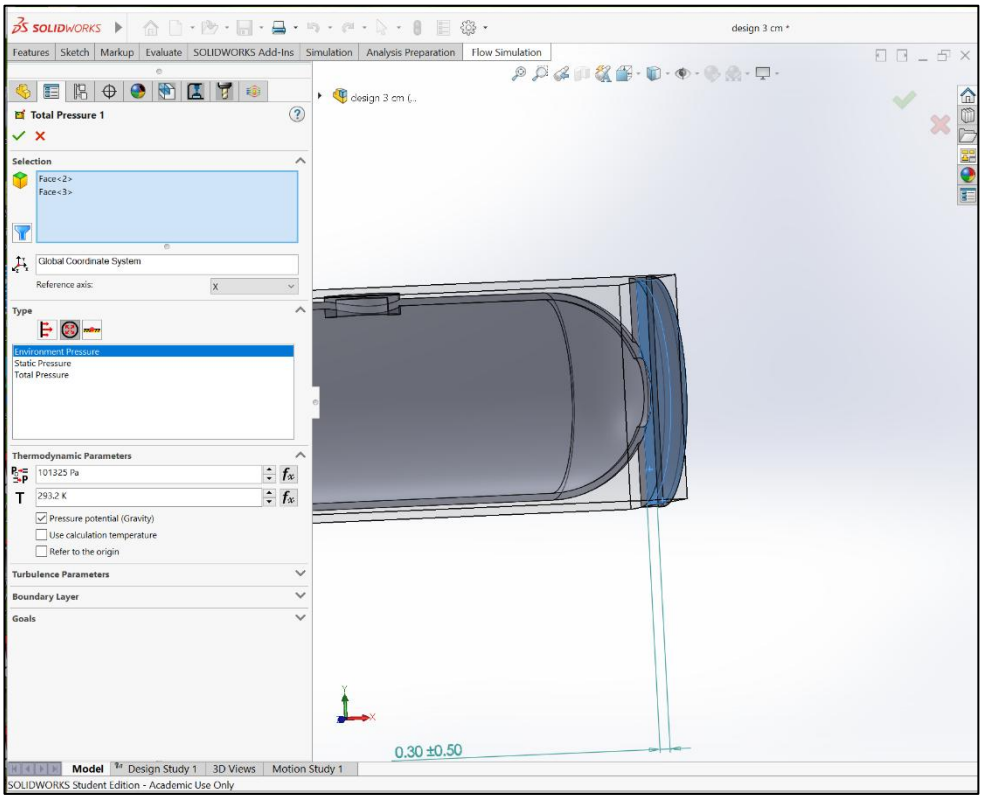

Figure 17: Defining Boundary Conditions at the inlet

3.5.5 Defining result parameters :

In the simulation setup, the key parameter of interest is the pressure sensor, referred to as **pu**. This parameter is monitored to evaluate the sensor's performance and response under different operating condition.

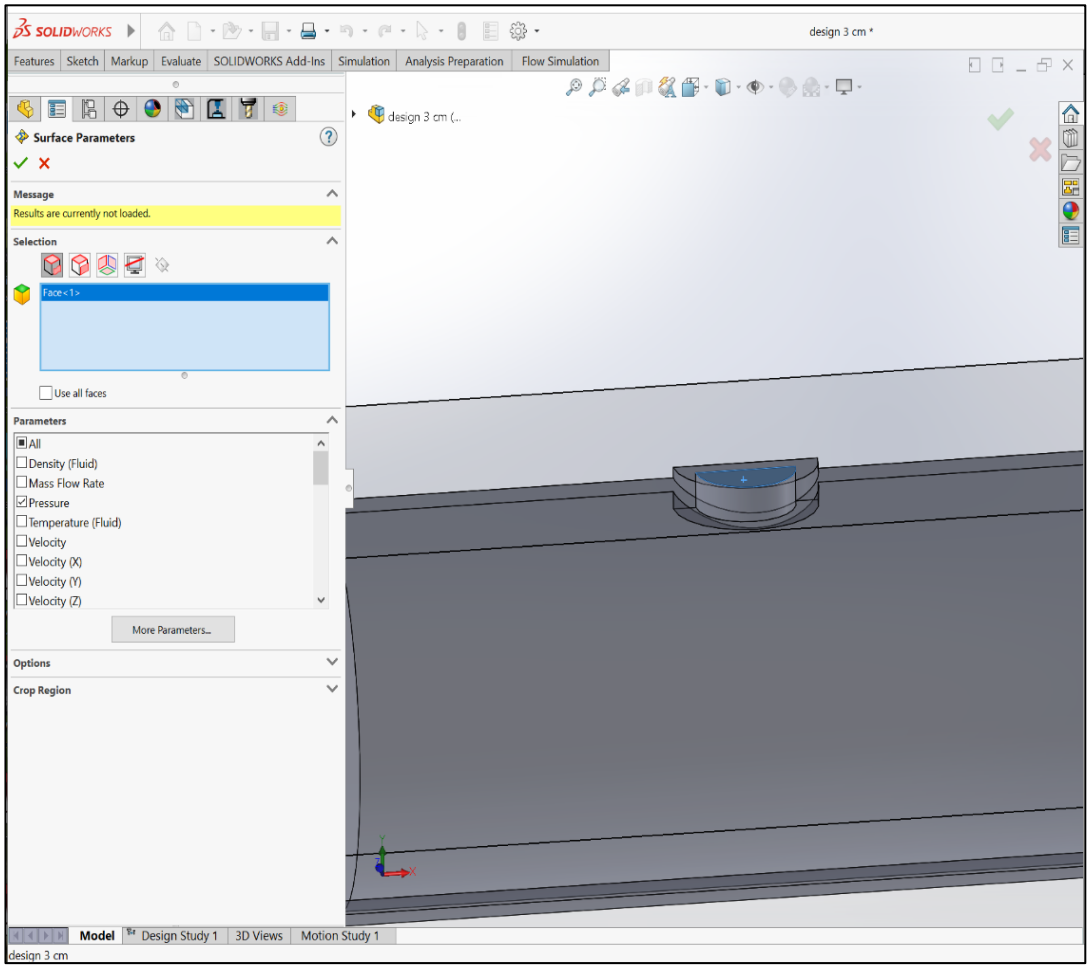

Figure 18:Inserting Parameters

3.5.6 Trajectory

Visualizing the flow trajectory as in Fig:19 lets us understand how the fluid moves through the system. This process helps reveal how the flow behaves along specific paths and how it interacts with different regions or obstacles. By examining these trajectories, it becomes possible

to identify critical areas such as high-pressure or low-pressure zones, which can guide design improvements to enhance the system's overall performance and efficiency.

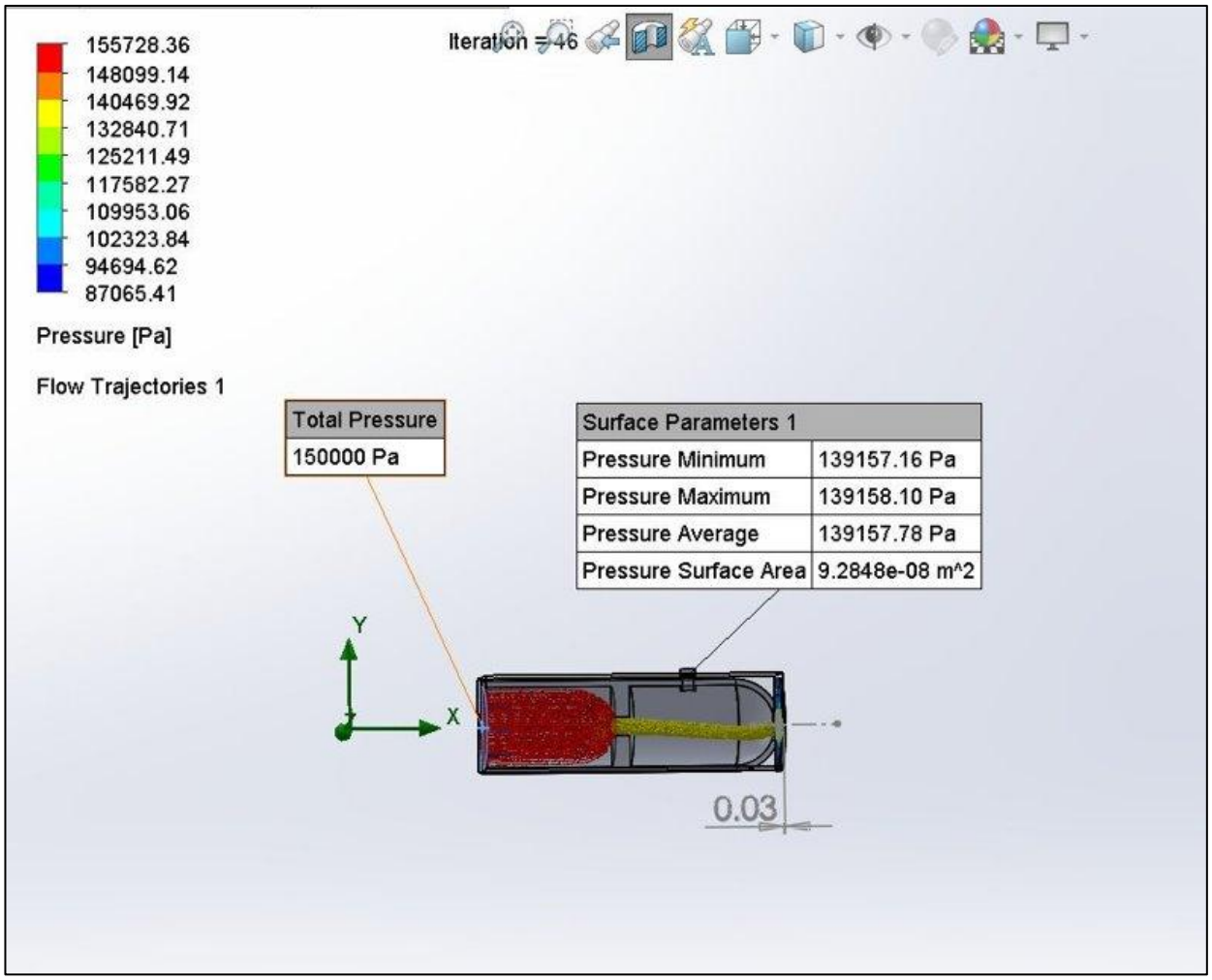

Figure 19:Flow trajectory

3.6 Methodology: Flow Simulation – Results and Curve Construction

Following the completion of the flow simulations, the pressure values at the Pressure Unit (PU) surface were recorded for each simulation scenario. These scenarios included various boundary conditions applied at the pressure inlet, as well as different axial distances between the

sensor port and the object being measured. The aim was to investigate how both inlet conditions and sensor positioning influence the pressure signal detected by the back-pressure sensor.

For every combination of inlet boundary condition and sensor-object distance, the PU pressure was extracted from the simulation results. This data was then systematically organized into a structured table for clarity and comparison. Each row in the table corresponds to a distinct simulation case, while the columns represent the inlet pressure condition, sensor distance, and the resulting PU pressure value.

To further interpret the results, Python was used to process the recorded data and generate graphical representations. Specifically, the PU pressure values were plotted as a function of the distance between the sensor and the object for each inlet pressure scenario. These plots enabled the visualization of characteristic curves that describe how the sensor's pressure reading responds to changes in position and boundary conditions. Each curve reflects a specific pressure inlet level, allowing for a direct comparison of the sensor behavior under varying flow intensities.

The resulting curves exhibited consistent trends, with PU pressure generally decreasing as the sensor was placed further from the object. This aligns with the physical expectation that flow interference and back-pressure effects diminish with increasing separation. Additionally, higher inlet pressures corresponded to proportionally higher PU readings across all distances, further validating the sensor's responsiveness.

These characteristic curves serve as valuable tools for both design calibration and practical sensor deployment. They offer insight into how the sensor should be positioned for optimal performance and help predict its output in different operational environments.

The flow simulations were performed for two different sensor housing designs, each characterized by distinct internal geometric parameters. In the first design, the internal dimensions

were set to 0.4 and 0.6 mm, while in the second design, the parameters were adjusted to 0.5 and 0.6 mm. These variations were introduced to assess how subtle changes in internal geometry influence the flow behavior and the pressure measured at the Pressure Unit (PU). For both designs, the same simulation procedure was followed, including identical boundary conditions and sensor-to-object distances, allowing for a direct comparison of performance between the two configurations.

3.6.1 Experimental Measurements Results of D1 0.4 and D2 0.6

Table 1:D1= Measurements Results of D1 0.4 and D2 0.6

x (mm)	P = 2 bar (Pa)	P = 3 bar (Pa)	P = 4 bar (Pa)	P = 5 bar (Pa)
0	200000	300000	400000	500000
0.015	195000	290000	387500	485000
0.03	190000	280000	375000	470000
0.045	180000	260000	337500	425000
0.06	170000	240000	300000	380000
0.075	152500	205000	255000	320000
0.09	135000	170000	210000	260000
0.105	125000	155000	177500	210000
0.12	115000	140000	145000	160000
0.135	112500	135000	142500	152500
0.15	110000	130000	140000	145000
0.165	109000	127500	139000	144000
0.18	108000	125000	138000	143000
0.195	108000	125000	138000	143500
0.21	108000	125000	138000	144000
0.225	108500	125500	138500	144500
0.24	109000	126000	139000	145000

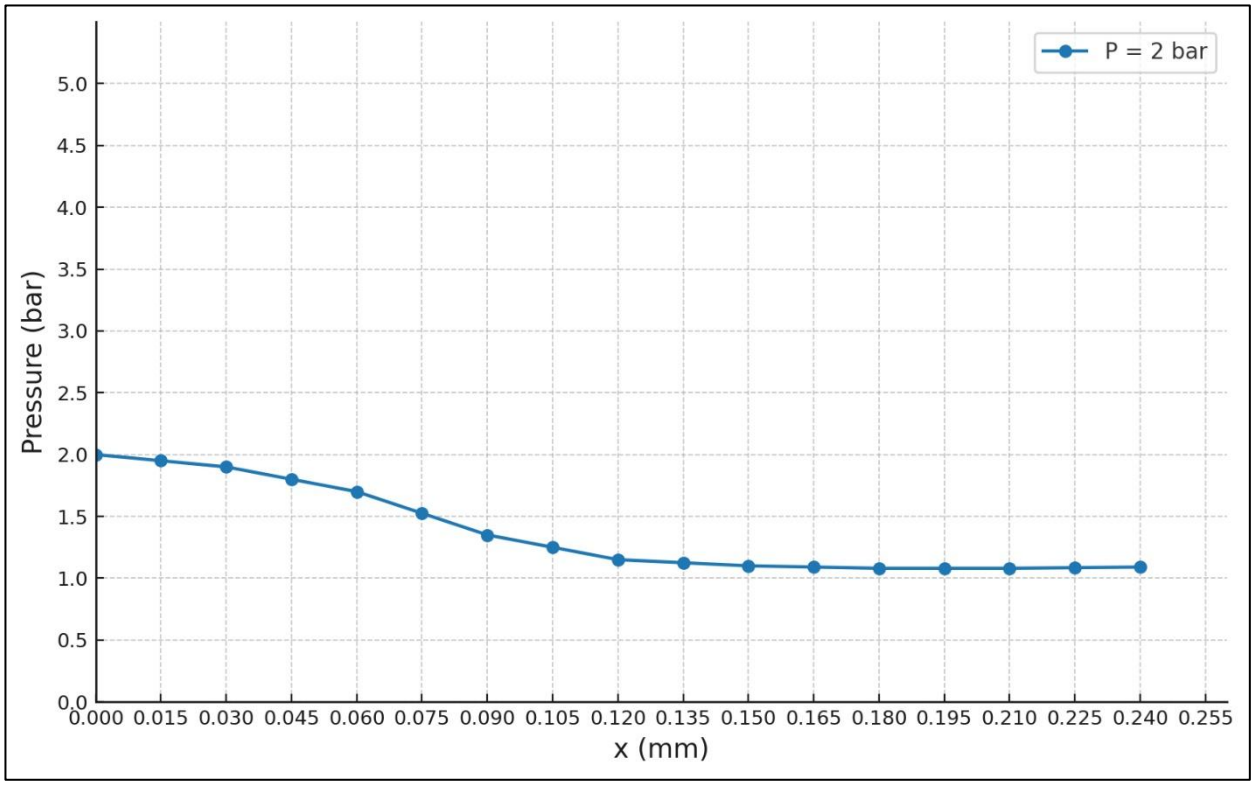

Figure 20:characteristic curve of D1=0.4 and D2 =0.6 at 2 bar

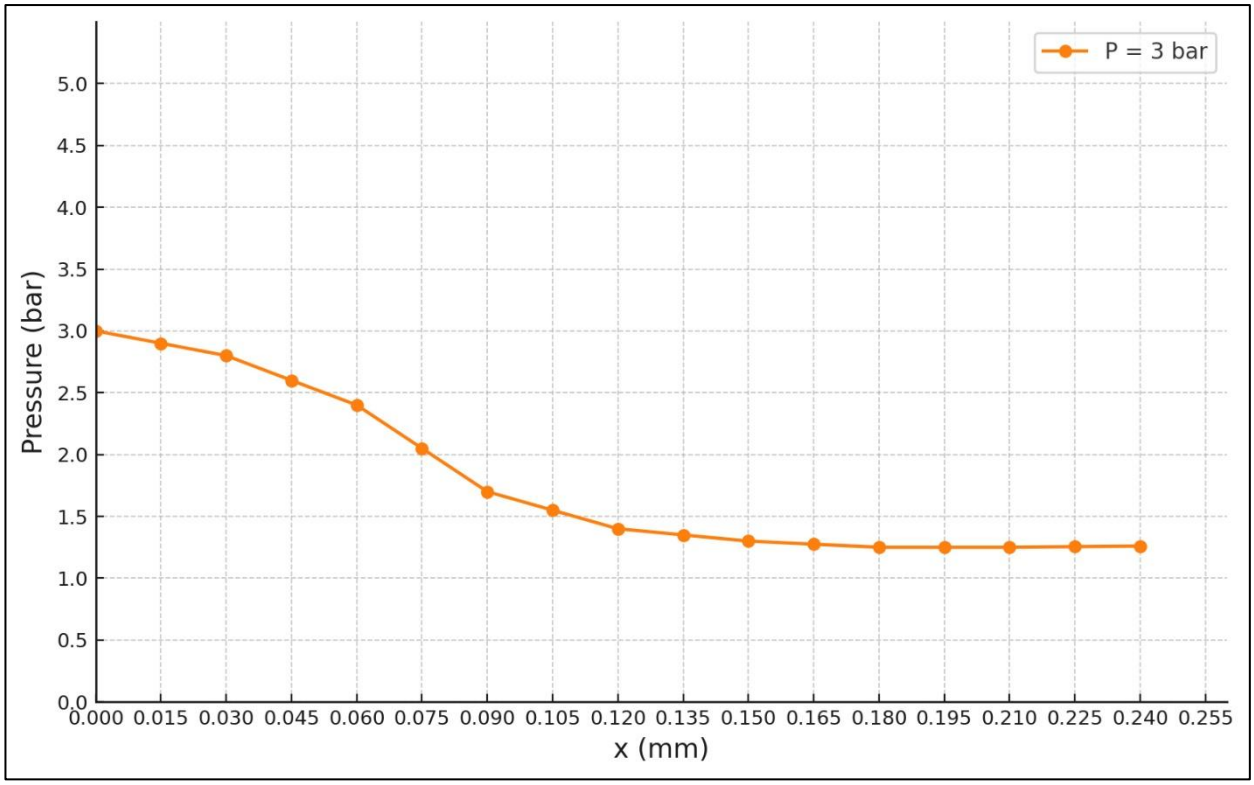

Figure 21: characteristic curve of D1=0.4 and D2 =0.6 at 3 bar

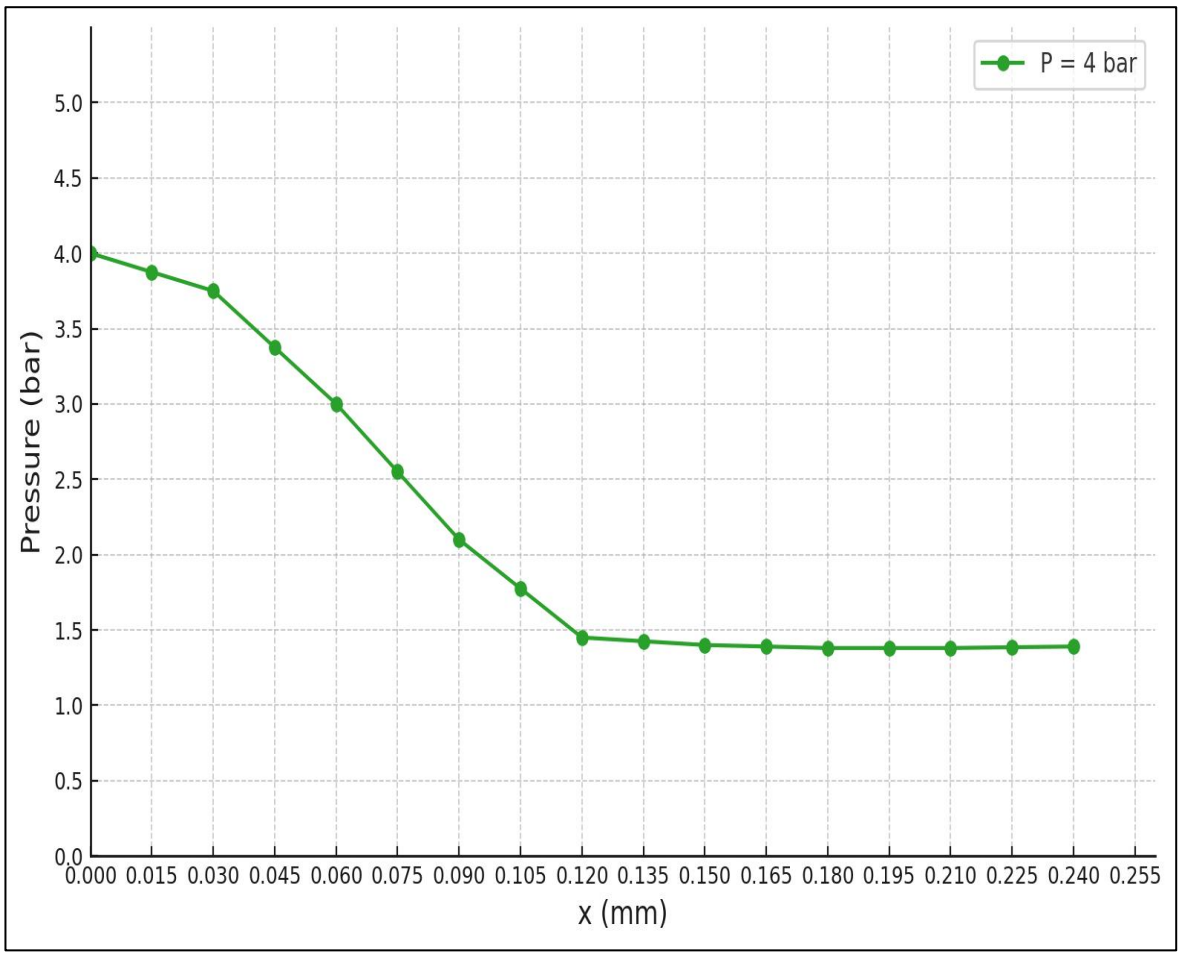

Figure 22: characteristic curve of D1=0.4 and D2 =0.6 at 4bar

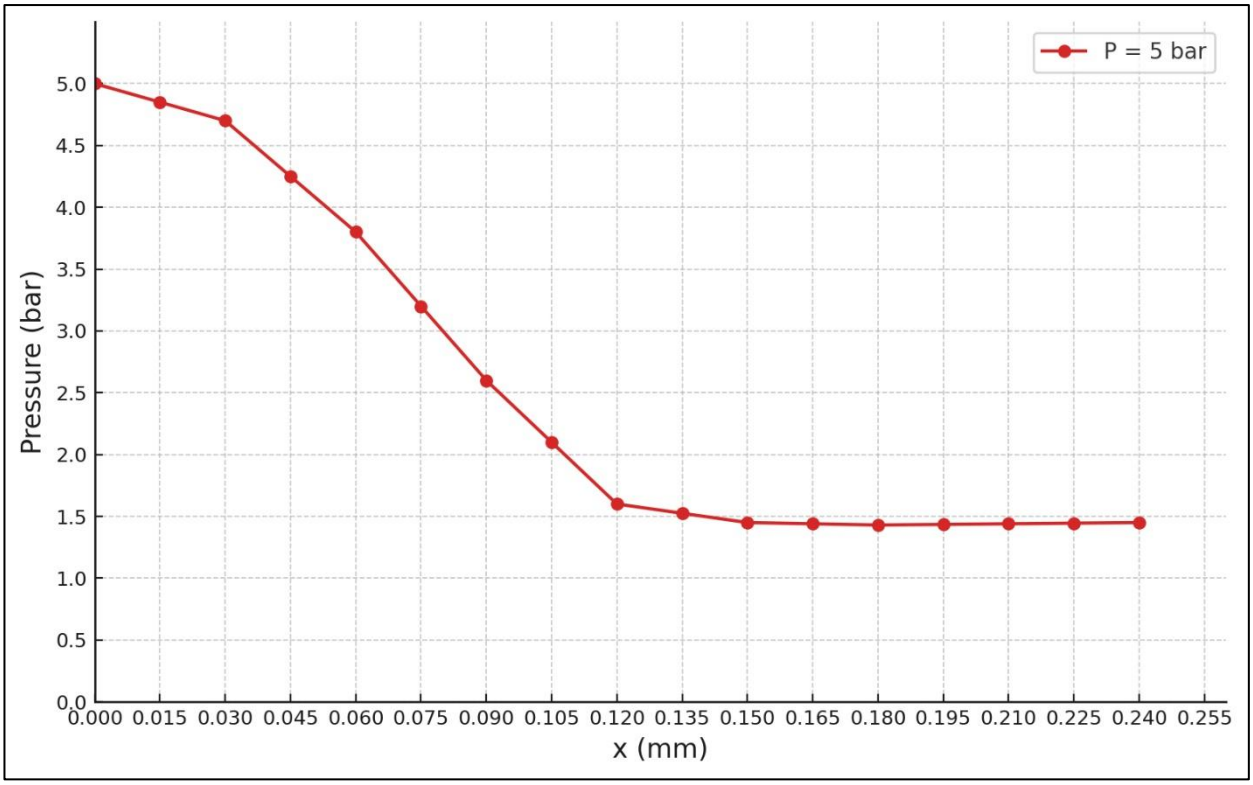

Figure 23: characteristic curve of D1=0.4 and D2 =0.6 at 5 bar

3.6.2 Experimental Measurements Results of D1 0.5 and D2 0.6

Table 2: Measurements Results of D1 0.5 and D2 0.6

x (mm)	P = 2 bar (Pa)	P = 3 bar (Pa)	P = 4 bar (Pa)	P = 5 bar (Pa)
0	2	3	4	5
0.015	1.975	2.95	3.925	4.925
0.03	1.95	2.9	3.85	4.85
0.045	1.9	2.825	3.775	4.75
0.06	1.85	2.75	3.7	4.65
0.075	1.75	2.55	3.425	4.275
0.09	1.65	2.35	3.15	3.9
0.105	1.625	2.3	3.05	3.75
0.12	1.6	2.25	2.95	3.6
0.135	1.575	2.225	2.9	3.575
0.15	1.55	2.2	2.85	3.55
0.165	1.525	2.175	2.825	3.525

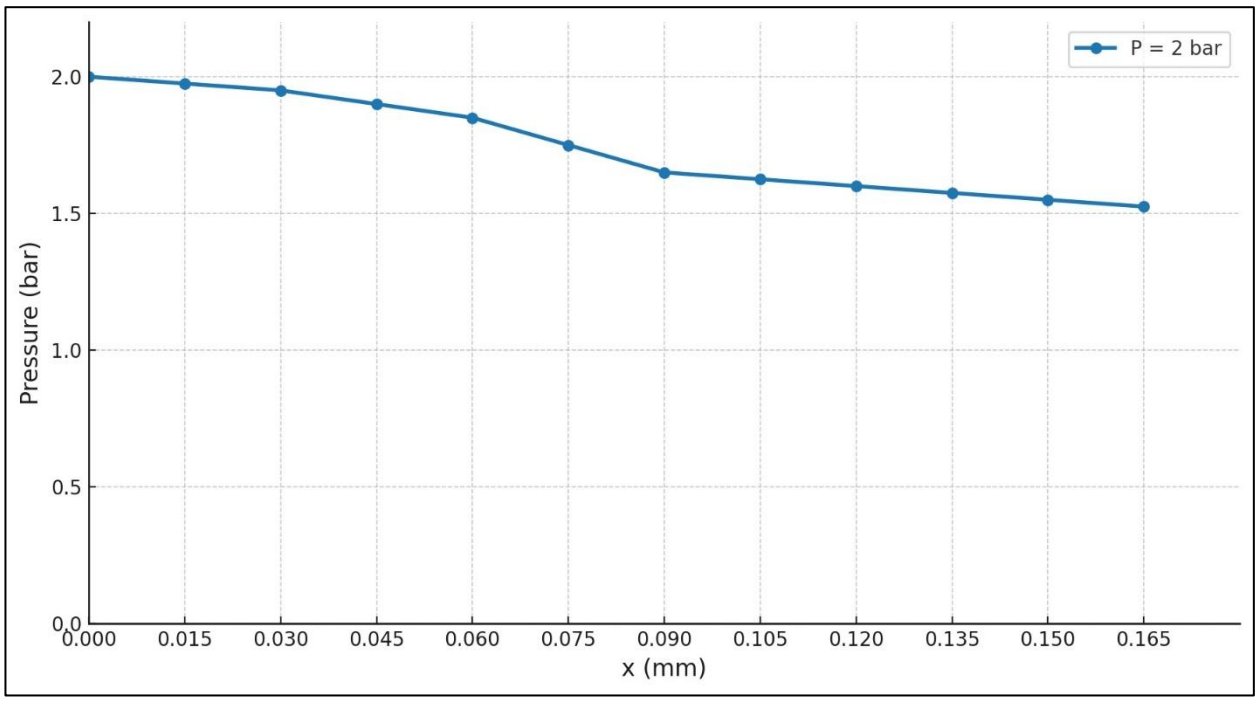

Figure 24:characteristic curve of D1=0.5 and D2 =0.6 at 2 bar

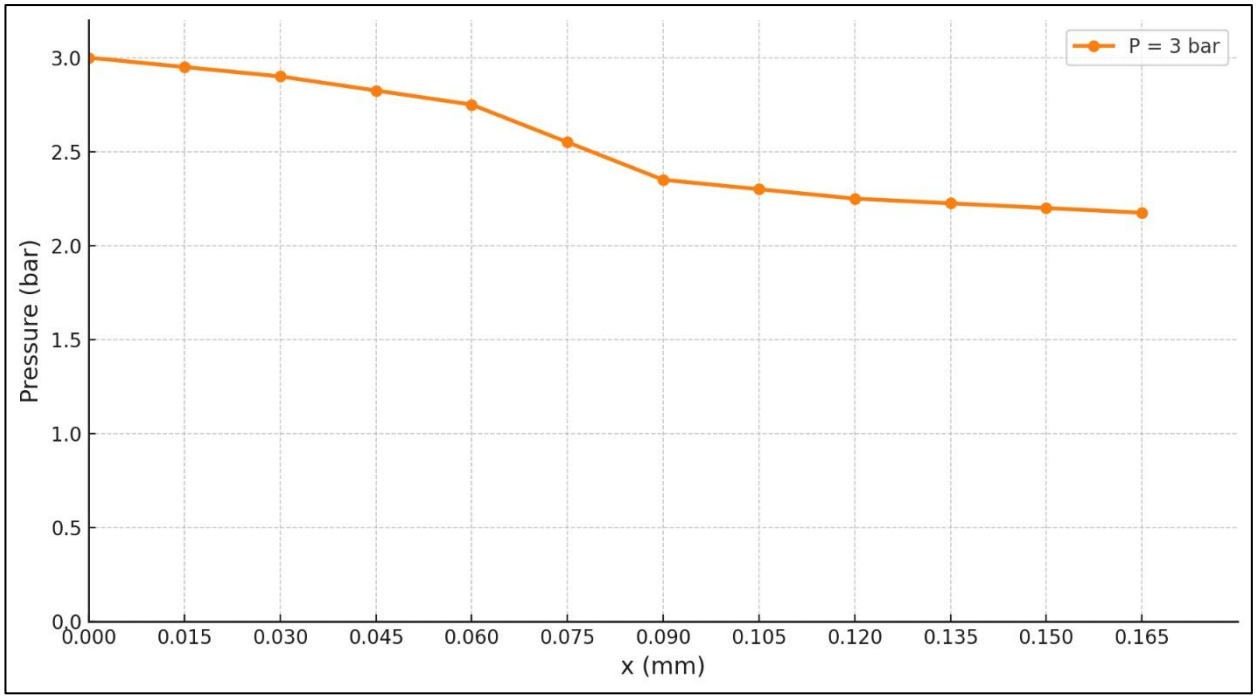

Figure 25: Figure 26:characteristic curve of D1=0.5 and D2 =0.6 at 3 bar

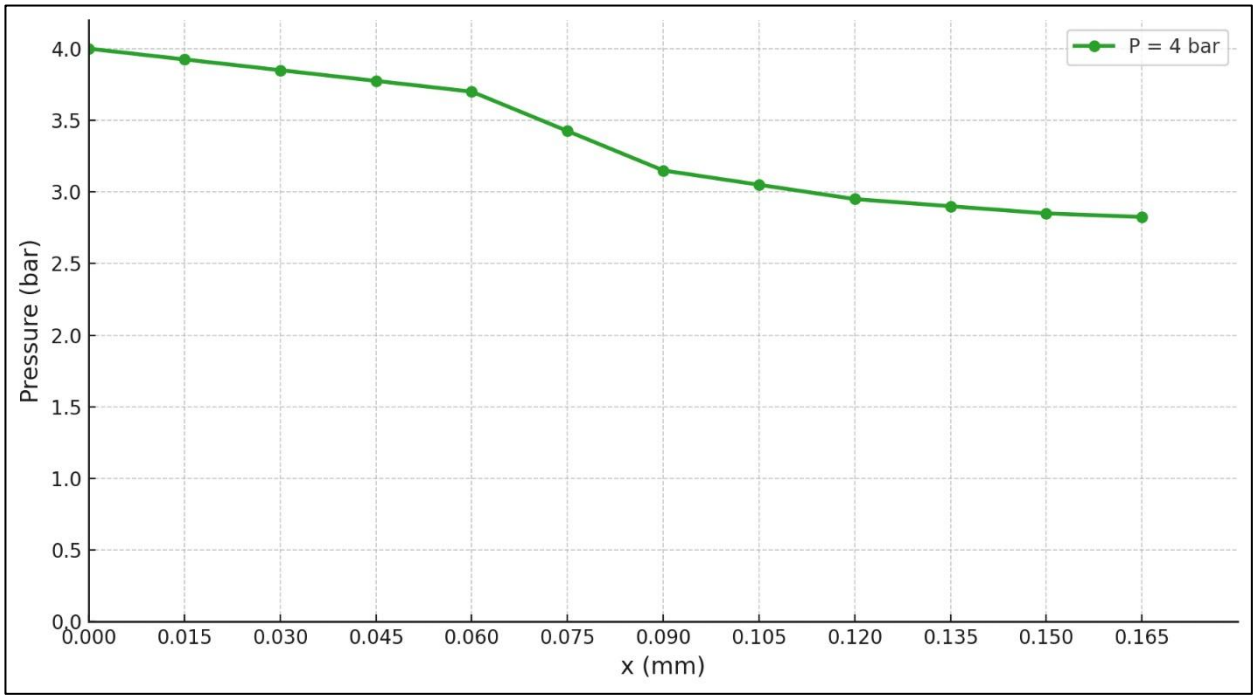

Figure 27: characteristic curve of D1=0.5 and D2 =0.6 at 4 bar

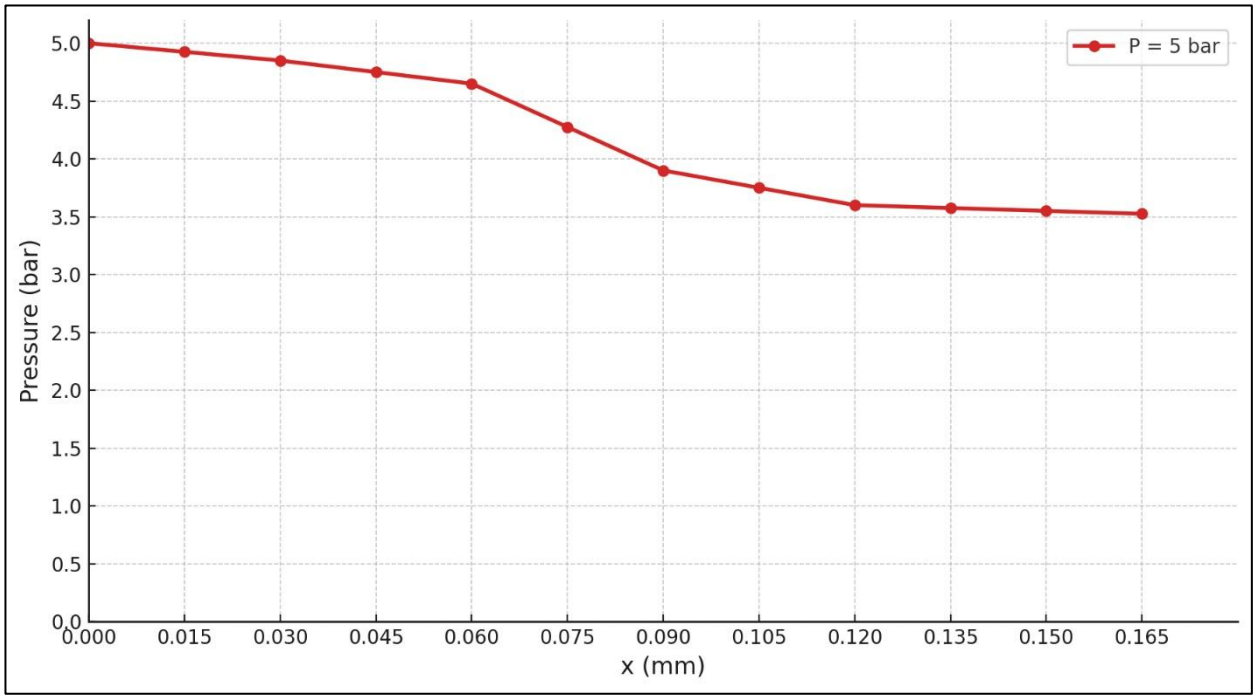

Figure 28:characteristic curve of D1=0.5 and D2 =0.6 at 5 bar

Chapter 4: Manufacturing Process

Following the completion of a comprehensive experimental analysis and the development of a detailed 3D model using SolidWorks, the project advanced to the physical development stage of the sensor. The virtual model served as a fundamental reference, providing the necessary framework for exploring suitable manufacturing methods to produce a functional prototype. The primary objective at this stage was to transform the digital design into a tangible device capable of being tested under real-world conditions.

This phase involved a careful assessment of various manufacturing technologies to identify those most compatible with the sensor's design specifications, material requirements, tolerance levels, and intended application. The main manufacturing methods considered were additive manufacturing (3D printing) and conventional machining. Each technique presented distinct advantages and limitations, which were evaluated in terms of design complexity, required precision, production feasibility, and the resources available.

4.1.1 Additive Manufacturing (3D Printing)

3D printing, also known as additive manufacturing, was one of the first fabrication methods we explored for building the sensor. This process creates parts layer by layer directly from the 3D CAD model, making it possible to produce complex shapes, reduce material waste, and speed up the prototyping process.

Using 3D printing allowed us to quickly create and test early versions of the sensor, helping us visualize the design and check how the components fit together. However, due to limitations in material strength and the precision of the printed parts, we decided that this method was not suitable for the final version of the prototype and began looking into other manufacturing options.

4.1.2 Subtractive Manufacturing (Machining)

Machining refers to a group of subtractive manufacturing processes—such as milling, turning, and drilling—where material is carefully removed from a solid block, usually metal or plastic, to create the desired shape. This method is widely used in industry and is known for its high precision and excellent surface finish.

For our project, we considered CNC (Computer Numerical Control) machining as one of the main options for producing the structural parts of the sensor. CNC machining offers several important advantages:

- **High Dimensional Accuracy:** CNC machines can achieve very tight tolerances, often within microns, which is essential for precision components like sensor housings or mounting brackets.
- **Material Flexibility:** A wide variety of materials can be used in machining, including metals like aluminum, stainless steel, and brass, as well as engineering plastics such as Delrin and PEEK—materials commonly used in sensor applications.
- **Durability and Strength:** Machined components generally have greater strength and durability compared to 3D-printed parts, particularly when subjected to mechanical loads or temperature variations.

Despite these clear advantages, machines also have some drawbacks. It is often more time-consuming and expensive, especially for complex shapes that may require multiple setups or custom tooling. Another concern is material waste, particularly when working with expensive raw materials.

In our case, CNC machining emerged as a strong choice for producing the final sensor housing and mounting parts, where high precision and mechanical robustness were critical.

For these reasons, we ultimately selected CNC machining for the fabrication of the final sensor components. This approach provided the necessary mechanical strength, precision, and long-term durability required for the sensor to perform reliably under real operating conditions.

4.2 Fabrication of Sensor Components Using CNC Machining

Once CNC machining was selected as the final manufacturing method, the fabrication of the sensor components began. This stage involved converting the finalized 3D models into machine-ready files, setting up the necessary machining operations, and carefully producing each part to meet the required dimensional accuracy and ensure reliable performance under real working conditions.

4.2.1 Preparation of CAD Models and Toolpaths

The design phase in SolidWorks concluded with the creation of detailed 3D assemblies of the sensor and its structural parts. These models were exported in STEP (.step) format, a widely used neutral file type that ensures compatibility between different CAD and CAM systems. This allowed the models to be imported smoothly into the CAM (Computer-Aided Manufacturing) software for the next steps.

For toolpath preparation, SolidWorks CAM was used to generate machining instructions. This process involved choosing the right cutting tools, setting the appropriate feed rates and spindle speeds, defining entry points, and planning the sequence of machining operations. The machining strategy for each part was carefully tailored to its complexity, taking into account critical dimensions, geometric features, and surface finish requirements.

4.2.2 Material Selection and Machining Overview

Aluminum was chosen as the material for the machined components because it offers an excellent balance of strength and lightness, along with good corrosion resistance and ease of machining. Additionally, it provides sufficient durability to withstand the sensor's operating pressure of up to 5 bar. The main parts produced:

- Part 1: Inlet Port
- Part 2: Nozzle part
- Part 3: Main Body
- Part 4: Sensor Interface part

Part 1: The sensor is composed of four main components, each contributing to its function of controlling the airflow path. Part 1 serves as the base and includes the M5 threaded hole where the pressurized air is introduced through a connected fitting. This part also provides the interface for the first sealing element: an O-ring is placed between Part 1 and Part 2 to ensure an airtight seal and prevent leaks at the joint. The parts are securely fastened using four M3 x 35 mm socket head screws (TCEI) along with matching hex nuts, providing structural stability to the assembly.

Part 2: is thinner in profile and includes a central hole that guides the air further into the system. This part is specially designed to hold one of six interchangeable discs, each with a different central hole diameter: 0.3 mm, 0.4 mm, 0.5 mm, 0.6 mm, 0.8 mm, or 1 mm. By using these varying diameters, we can create different flow conditions for comparative testing. The ability to easily

swap out discs makes Part 2 a critical element in controlling and adjusting the airflow characteristics.

Part 3: Positioned after Part 2, Part 3 features two O-rings—one on each side—to maintain a tight seal with adjacent parts. This component includes a 5 mm through-hole , guiding the airflow precisely to the digital manometer. In addition, Part 3 contains a side-mounted M5 hole connected to a secondary outlet. This allows a portion of the pressurized air to escape in a controlled manner, while the remaining flow continues toward the final section of the sensor. This controlled diversion is essential for fine-tuning the pressure at the sensing surface.

Part 4: acts as the final disk in the sensor and includes a central hole through which the air exits. Like Part 2, this component can be fitted with one of six interchangeable discs, matching the same set of diameters (0.3 mm to 1 mm). This allows for multiple combinations of inlet and outlet restrictions, enabling detailed analysis and optimization of sensor performance. Part 4 also includes the M3 screw heads used to hold the entire assembly together, completing the sensor structure. The airflow that exits from this part is used to determine the distance to the target surface based on pressure variation, forming the basis of the sensor's measurement function.

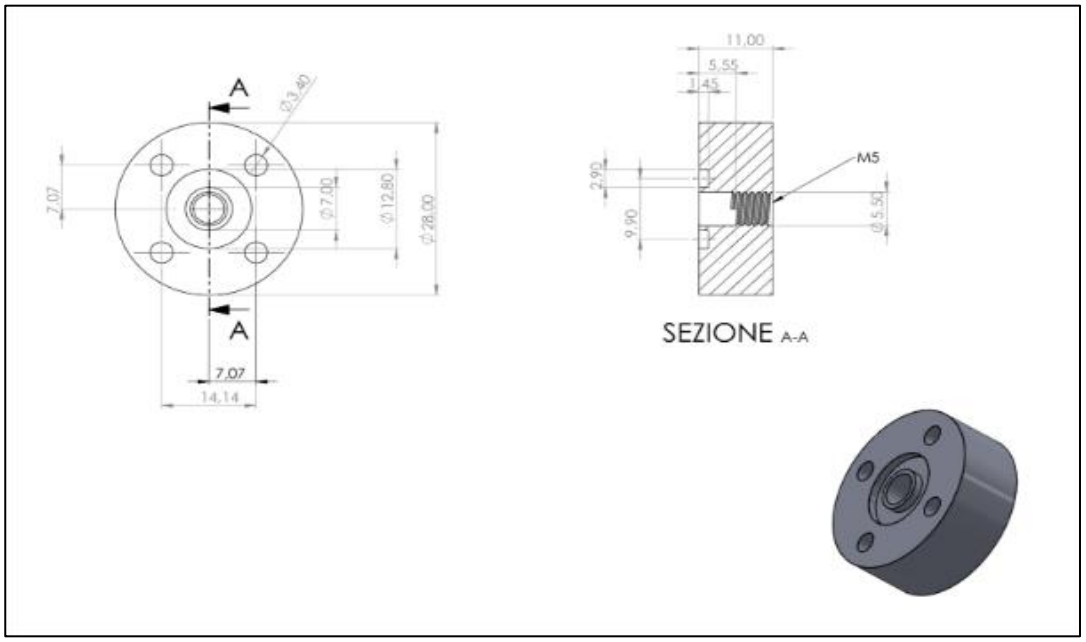

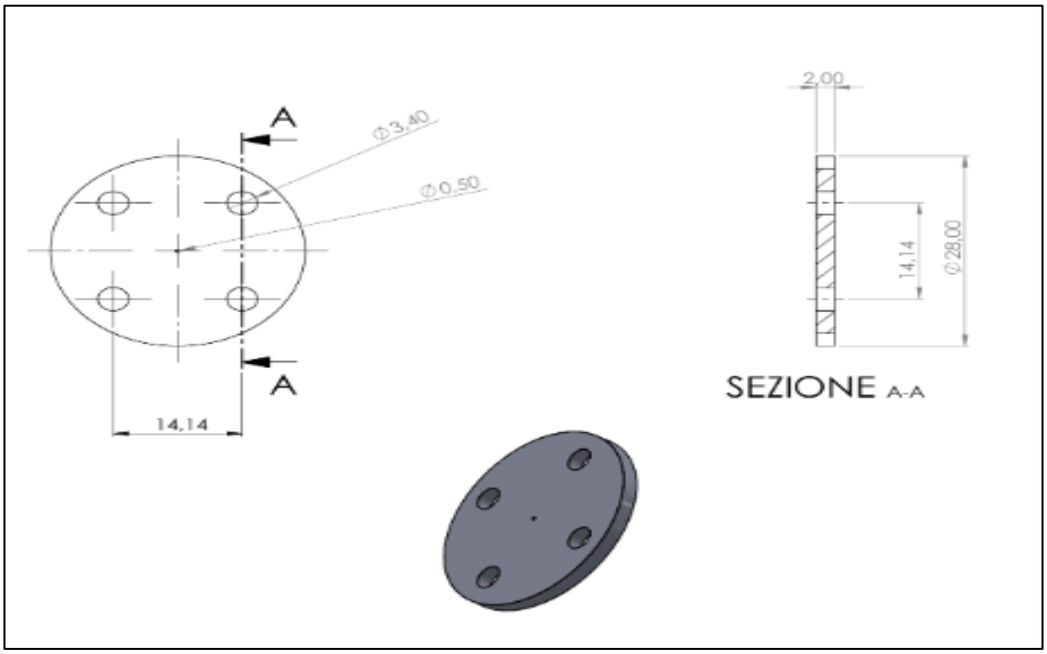

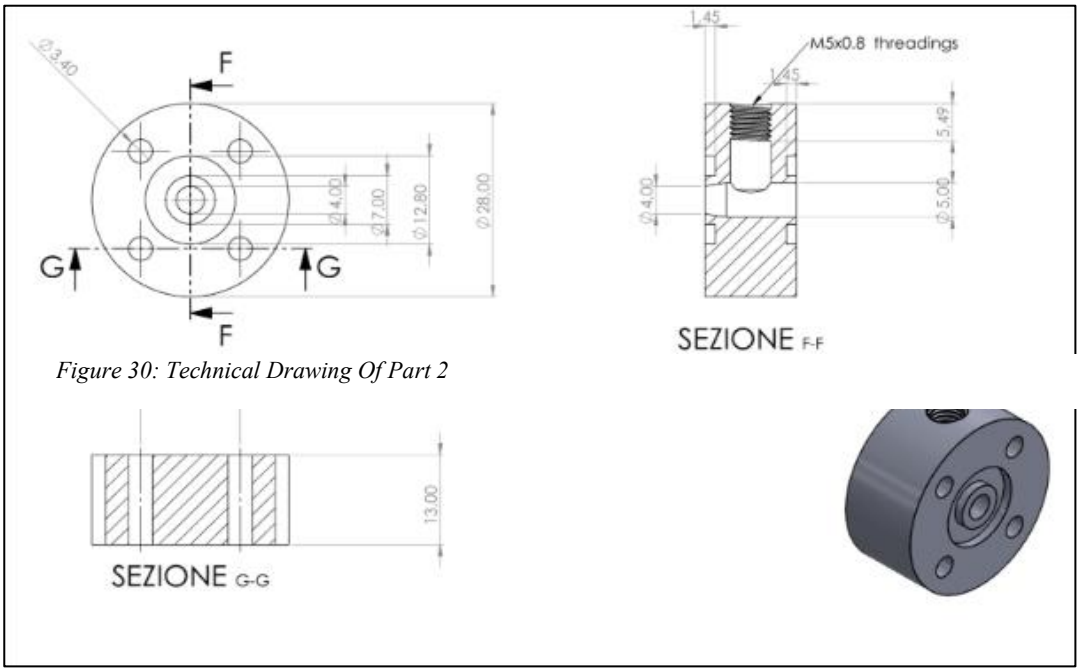

Figure 30: Technical Drawing Of Part 2

Figure 31: Technical Drawing Of Part 3

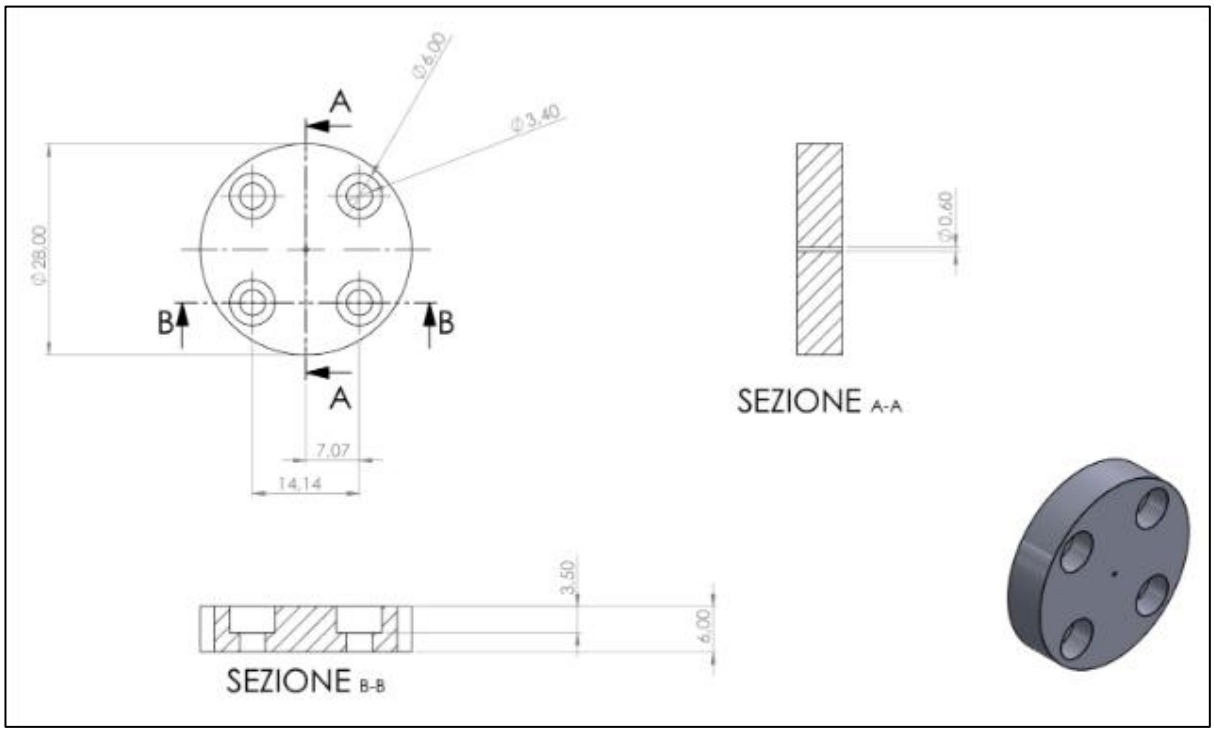

Figure 32: Technical Drawing Of Part 4

4.2.3 Quality Control and Dimensional Verification

Upon completion of the machining process, all critical dimensions were carefully inspected using calibrated measuring instruments, including digital calipers, micrometers, and depth gauges. Particular attention was given to several key aspects:

- The precise alignment of holes and internal channels
- The quality and depth of threaded features
- The uniformity of wall thickness in pressurized areas
- The flatness and perpendicularity of mating surfaces

To ensure proper assembly and reliable performance, dimensional tolerances were maintained within ±0.05 mm, especially in regions where sensor elements or sealing components would be installed. Components that did not meet these tolerance requirements were either re-machined to achieve compliance or excluded from the final assembly to maintain overall quality and functionality.

4.2.4 Post-Machining Processes

Following the completion of machining, the components underwent a series of post-processing steps to prepare them for assembly and ensure their functionality and durability:

- **Deburring:** Manual deburring was carried out using files and abrasive tools to remove any sharp edges and metal burrs left from machining. This step was essential to ensure safe handling and proper assembly of components.
- **Surface Cleaning:** All parts were thoroughly cleaned using alcohol to remove machining oils, metal shavings, and other residues, leaving the surfaces clean and free of contaminants.

- **Thread Inspection and Reinforcement:** The threaded holes were carefully inspected and tested to confirm proper fit. In critical locations, helicoil inserts were installed to strengthen the threads, enhancing their resistance to wear and increasing durability, particularly in areas subject to repeated assembly and disassembly.
- **Surface Finishing:** To improve both the appearance and corrosion resistance of the aluminum parts, optional surface treatments such as anodizing or clear protective coatings were applied

4.3 Assembly and Integration

After the successful fabrication of the individual components through CNC machining, the next phase focused on assembling these parts into a complete sensor unit. This assembly process played a crucial role not only in verifying the proper fit and function of each component but also in ensuring the mechanical integrity, effective sealing, and precise alignment of the sensor—factors essential for accurate and reliable data acquisition.

4.3.1 Component Preparation

Before assembly, all machined components were carefully inspected to ensure cleanliness and dimensional accuracy. O-rings, fasteners, sealing materials, and sensor elements were also prepared in advance. Special attention was given to keeping the sensor cavity free from dust or debris that could affect performance.

Threaded connections were cleaned and lubricated as needed, while all sealing surfaces were checked for imperfections. Any defects that might compromise pressure integrity were corrected through polishing or by replacing the affected parts.

3.3.2 Assembly Procedure

The assembly of the sensor was carried out step by step to ensure proper alignment, sealing, and functionality:

- **Housing and Sensor Element Installation:**

  The machined aluminum housing served as the main body, with the sensor element carefully installed in its designated cavity. Precision alignment features ensure correct positioning.

- **O-Ring Choosing:**

  High-quality O-rings were installed at all interface joints to ensure a reliable, leak-proof seal. The O-ring grooves were carefully machined within standard tolerances to achieve the right level of compression without overstressing the material. In designing the grooves, we considered the internal diameter of the sensor, which is 5.5 mm, and the external diameter of 20 mm which revlead in Fig:28, while also making space for M3 bolts. Based on the O-ring manufacturer's datasheet, we selected a 2:9 mm O-ring as the most suitable option. The groove dimensions were then designed accordingly, following the specifications provided in the datasheet to ensure proper fit and sealing performance. And according to that we choose Fig 7 From data sheet as correspondence design which is face sealing so that we need to do groove depth h=1.4, and l1=1.45mm to make sure that o ring close well and not make problems.

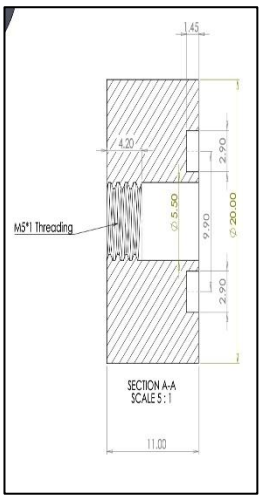

Figure 33:Technical Drawing Showing Internal Diameter

GENERAL TECHNICAL INFORMATION

MAX SPARE LIMITED
QUALITY. PRECISION. SPEED.

SEAL HOUSING DIMENSIONS, TOLERANCES AND DESIGN CRITERIA FOR STANDARD APPLICATIONS

Design criteria are based on the elastomeric compound of 70 Shore A, working at pressure up to 10 Bar and temperature between -30°C and +100°C. For other working conditions (pressures, temperature, etc) it may be necessary to select elastomeric compounds of other hardness or to incorporate anti-extrusion rings.

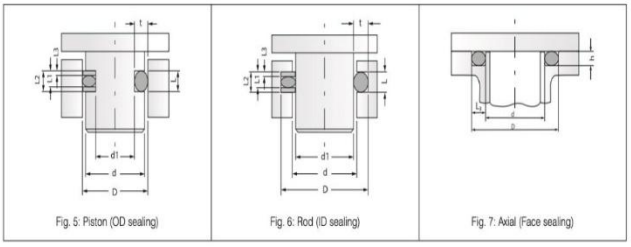

Fig. 5: Piston (OD sealing) | Fig. 6: Rod (ID sealing) | Fig. 7: Axial (Face sealing)

Table 1: O-Ring housing dimensions for piston, rod & axial staling.

O-Ring C/S	Preferred Diameters Range d/D	Groove Depth		Groove Width L +0.20		Groove Width 1 Backup Ring L1 + 0.25 5 & 6	Groove Width 2 Backup Ring L2 + 0.25 5 & 6	Backup Ring Width L3
		Fig. 5 & 6 (t)	Fig. 7 (h) +0.10 -0.00	Fig. 5 & 6	Fig. 7 (L3)			
1.00	1-10	0.80	0.75	1.40	1.60	2.40	3.40	1.00
1.50	10-15	1.20	1.10	2.00	2.20	3.00	4.00	1.00
1.78	15-20	1.35	1.25	2.40	2.60	3.40	4.40	1.00
2.00	20-50	1.55	1.45	2.70	2.90	3.70	4.70	1.00
2.50	20-50	1.95	1.85	3.40	3.60	4.90	6.40	1.50
2.62	20-50	2.00	1.90	3.60	3.80	5.10	6.60	1.50
3.00	50-80	2.35	2.25	4.10	4.30	5.50	7.00	1.50
3.50	50-80	2.75	2.65	4.80	5.00	6.30	7.80	1.50
3.53	50-80	2.80	2.70	4.80	5.00	6.50	7.80	1.50
4.00	80-250	3.20	3.10	5.30	5.50	6.80	8.30	1.50

Figure 34:Oring Data sheet

- **Attachment of End Caps or Covers:**

  Covers were aligned using dowel pins where necessary and secured with stainless steel screws. A torque wrench was used to tighten the screws evenly, ensuring uniform pressure on the seals and preventing distortion.

- **Mounting Brackets and Supports:**

  Sensor placed inside the support securely during testing. These supports were precisely machined to provide stability while allowing for fine adjustments.

- **Wiring and Connector Integration:**

  Electrical connections were completed using soldering or terminal blocks, with careful routing of wires to prevent mechanical stress or interference. Strain relief and protective tubing were added where necessary to enhance durability.

4.3.3 Testing During Assembly

Several preliminary tests were carried out during the assembly to identify and resolve any immediate issues:

- **Leak Testing:**

  Compressed air and a soap solution were used to check for leaks at joint lines, with the appearance of bubbles indicating sealing problems.

- **Electrical Testing:**

  Continuity and signal integrity tests were performed to verify proper wiring and ensure that connectors were functioning correctly.

- **Mechanical Fit Checks:**

  The mechanical fit of all components was checked to confirm smooth assembly and

proper alignment. Fasteners were tightened to the specified torque without any signs of misalignment or distortion.

4.4 Assembly and Final Sensor Components

After completing the individual part manufacturing through CNC machining, all components were assembled to create the final sensor unit. The figures below illustrate the fully assembled sensor.

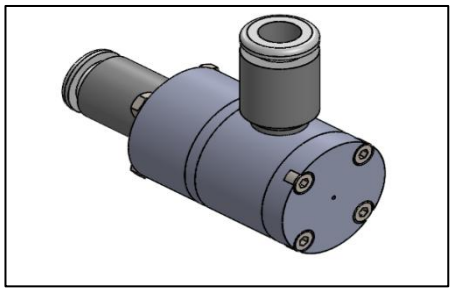

Figure 35: Fully Assembled Sensor System

4.4.1 Sensor Assembly on the Test Bench

After the successful manufacturing and assembly of all components, the sensor was integrated into the test bench for validation and calibration. The test bench was prepared to replicate the pressure conditions the sensor would encounter during operation. All mechanical connections, including threaded fittings and support brackets, were carefully installed to ensure a secure and leak-free setup. Electrical connections were completed by wiring the pressure transducer to the data acquisition system and powering the digital manometer.

This stage was essential for verifying the sensor's performance in a controlled environment. The integration process confirmed the mechanical compatibility of the fabricated components and validated the overall design before proceeding to data collection.

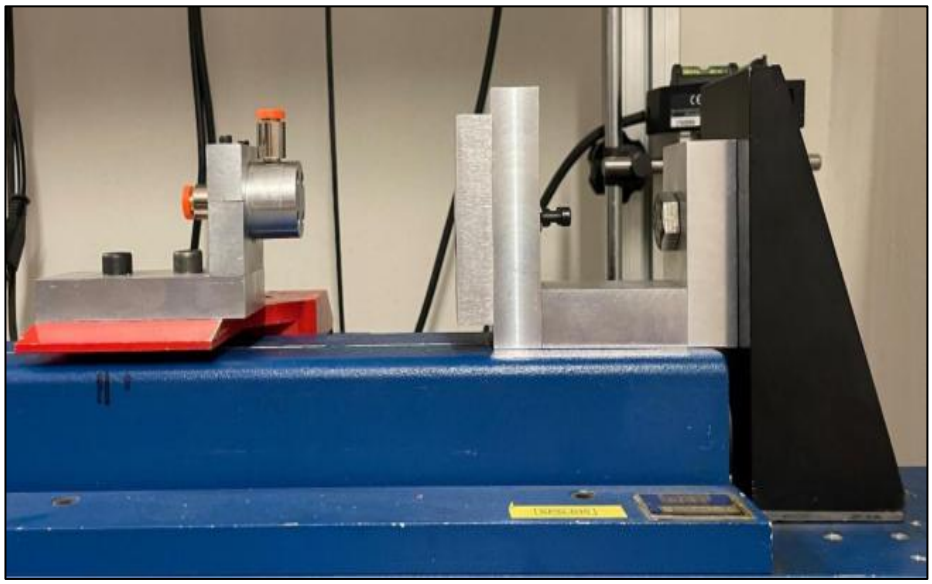

Figure 36: Assembled Sensor Mounted on the Test Bench (Front View)

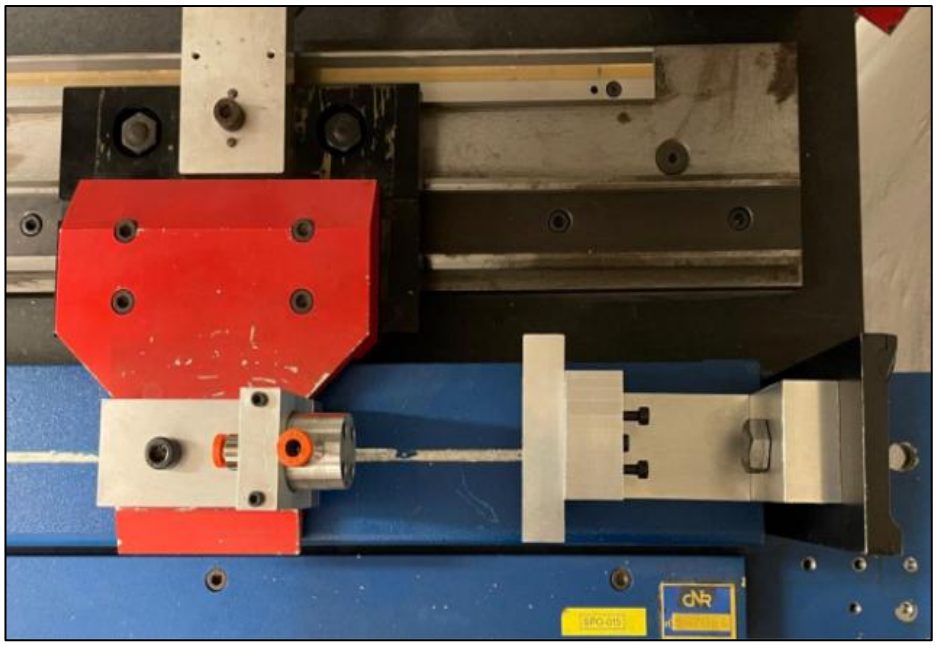

Figure 37: Assembled Sensor Mounted on the Test Bench (Top View)

This setup served as the foundation for the calibration and performance testing described in Chapter 5.

Following the setup of the apparatus, the air supply is connected along with the air sensor, manometer, and transducer. These instruments are essential for monitoring and recording pressure variations throughout the experiment. Once all components are securely in place and properly calibrated, the system is ready to initiate the experimental procedure.

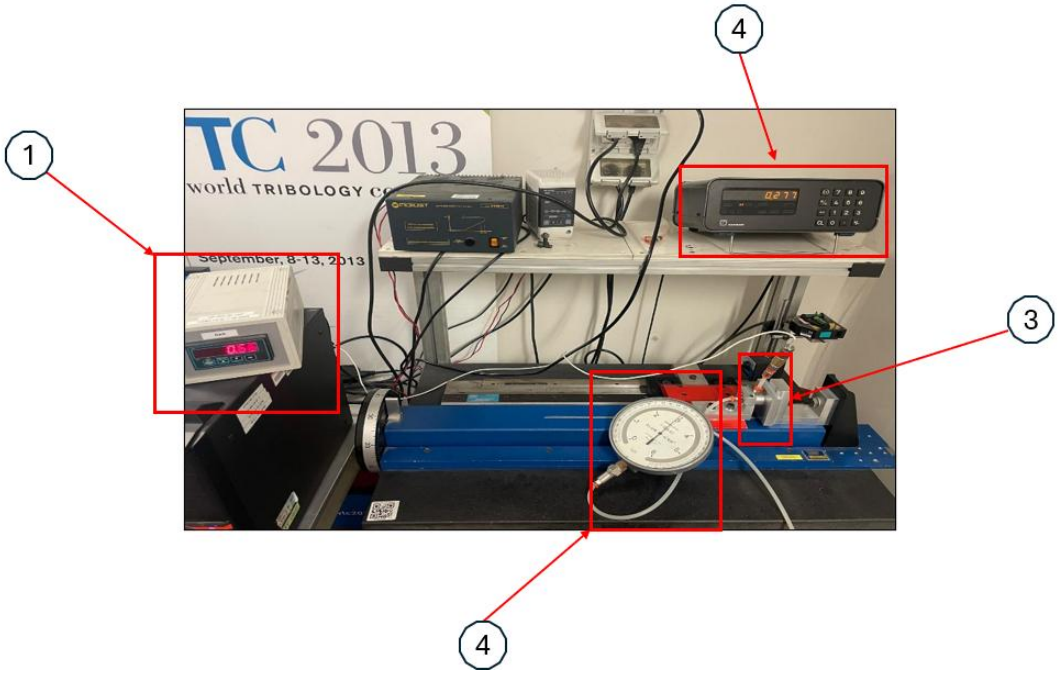

Figure 38:Sensor Mounted on test bench

1-Trancducer

2-Manometer

3-Sensor

4-Distance indicator

\

Chapter 5: Testing and Validation

Sensor Assembly and Testing

Once the sensor was successfully assembled and all mechanical, pnumatic and electrical connections were checked and secured, the prototype was ready for testing. The goal of this phase was to assess the sensor's performance in controlled conditions, verify its accuracy, and ensure both its structural integrity and proper functioning. The testing process began with the calibration of pressure measurement devices to provide a reliable reference for all subsequent measurements.

5.1 Calibration of Pressure Gauges

Two pressure gauges were used during the testing: a digital manometer and a traditional analog (mechanical) manometer. Both were connected in parallel to the same pressure source, allowing for a direct comparison of their readings. This calibration step was essential to ensure that the measurement system was accurate and trustworthy before using it to evaluate the sensor output.

The calibration process was carried out in two stages. In the first stage, pressure gradually increased from 0 to 5 bar in increments of 0.5 bar, with the analog manometer serving as the reference. At each pressure step, the reading from the digital manometer was recorded. After reaching 5 bar, the pressure was slowly reduced back to 0 bar, again in 0.5 bar steps, with the digital readings recorded at each level.

In the second stage, the digital manometer was used as the reference. The same procedure was followed: pressure was increased and then decreased step by step, while the readings from the

analog manometer were carefully noted. This two-way calibration ensured that both instruments provided accurate and consistent results before proceeding to the sensor performance evaluation.

5.2.1 Results of Calibration and Data Analysis

After assembling and setting up the sensor, a thorough calibration process was carried out to evaluate the pressure transducer's response and accuracy. The main objective was to compare the readings from the digital transducer with those of a reference analog manometer while varying the pressure in a controlled manner.

The calibration involved both increasing and decreasing the pressure between 0 and 5 bar. Pressure was adjusted in steps of 0.5 bar, and at each step, readings from both the manometer and the transducer were recorded simultaneously. The same procedure was followed in reverse during the pressure release phase, with measurements taken at each level.

This approach allowed for the identification of any hysteresis or offset that could affect the transducer's performance, ensuring the reliability and consistency of the sensor output. The recorded data are presented in Table 3.

Table 3: ***Calibration Results of the Pressure Sensor***

Manometer (Up) [bar]	Transducer (Up) [bar]	Manometer (Down) [bar]	Transducer (Down) [bar]
0.0	0.03	0.0	-0.04
0.5	0.49	0.5	0.53
1.0	1.10	1.0	1.03
1.5	1.50	1.5	1.51
2.0	2.18	2.0	2.01
2.5	2.54	2.5	2.54
3.0	2.98	3.0	3.04
3.5	3.32	3.5	3.52
4.0	4.09	4.0	3.94
4.5	4.61	4.5	4.47
5.0	5.10	5.0	4.99
4.5	4.58	4.5	4.45
4.0	4.05	4.0	3.86
3.5	3.52	3.5	3.45
3.0	3.01	3.0	2.85
2.5	2.52	2.5	2.47
2.0	2.05	2.0	1.95
1.5	1.57	1.5	1.50
1.0	1.02	1.0	1.01
0.5	0.50	0.5	0.52
0.0	0.108	0.0	-0.03

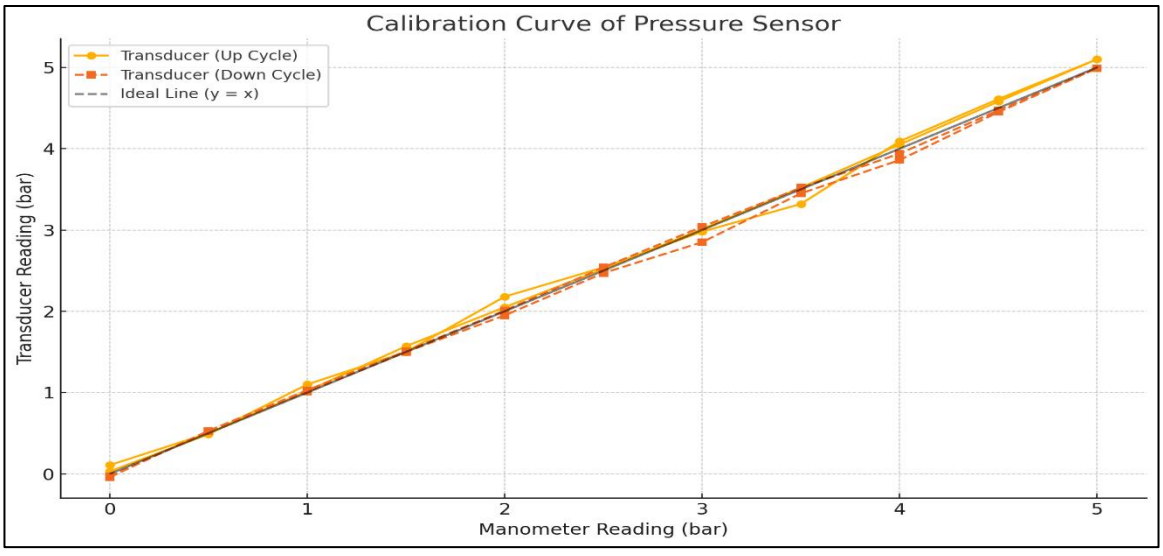

Figure 39: Calibration Curve of the Pressure Sensor (Comparison of Up and Down Cycles)"

5.2.2 Analysis of Calibration Results

Based on the calibration data, several key observations regarding the performance of the pressure transducer can be identified:

Linearity

The transducer demonstrated a clear linear relationship between applied pressure and output response during both the increasing and decreasing pressure cycles. As the pressure was raised from 0 to 5 bar, the transducer's output increased proportionally, with only minor deviations observed. This behavior confirms the sensor's ability to maintain linearity across its full operating range.

Accuracy and Offset

A slight offset was detected at 0 bar, where the transducer indicated approximately 0.03 bar during the increasing pressure cycle and -0.04 bar during the decreasing cycle. This minor discrepancy is likely attributable to small zeroing inaccuracies or internal electronic noise. Similarly, at the maximum pressure of 5 bar, the transducer readings slightly exceeded the reference values, recording 5.10 bar on the increasing cycle and 4.99 bar on the decreasing cycle. This corresponds to a marginal gain error of approximately 2%, which remains within the acceptable limits for typical engineering applications.

Hysteresis

A comparison of the transducer outputs during the pressure increases and decrease phases revealed small variations, indicating the presence of hysteresis. For example, at a nominal pressure of 4.5 bar, the sensor reported 4.61 bar during the increasing cycle and 4.45 bar during the decreasing cycle. The observed hysteresis is relatively minor and falls within standard engineering tolerances for pressure sensors of this type.

Repeatability

The sensor exhibited good repeatability, with consistent readings obtained across both pressure cycles. Variations at each pressure point were minimal, and the output followed a predictable pattern, demonstrating the sensor capability to deliver stable and reliable measurements under repeated testing conditions.

Sensitivity

The transducer responded consistently to each 0.5 bar change in applied pressure, with output variations closely matching those of the reference analog manometer. This level of sensitivity confirms the sensor's ability to detect and reflect incremental pressure changes with sufficient accuracy, rendering it suitable for a range of monitoring and control applications.

5.23 Conclusion of Calibration

The calibration results show that the pressure transducer performs reliably within the 0–5 bar range. The sensor demonstrates a clear linear response, acceptable levels of hysteresis, and consistent repeatability across both increasing and decreasing pressure cycles. The small offsets observed can easily be corrected using a simple linear calibration if higher precision is needed. Overall, these results indicate that the sensor is well-suited for use in the application.

5.3 Sensor Performance Testing

Following successful calibration, the sensor was ready for functional testing under controlled pressure conditions. This stage aimed to evaluate the accuracy, stability, repeatability, and response behavior of the sensor when subjected to varying pressures, similar to those expected in its intended application.

The testing process involved gradually applying pressure to the system while continuously recording output values from the pressure transducer. These readings were compared to a reference (the digital manometer) to assess performance metrics such as linearity, hysteresis, and any observed offset or drift. Multiple pressure cycles were conducted to confirm consistency and repeatability.

The results obtained from these tests are presented and analyzed in the following sections.

4.3.1 Experimental Measurements Results of D1 0.5 and D2 0.6

Table 4: Experimental Measurements Results of D1 0.5 and D2 0.6

X (mm)	Pressure 2 (BAR)	Pressure 3 (BAR)	Pressure 4 (BAR)	Pressure 5 (BAR)
0.0	1.93	2.82	3.85	4.83
0.015	1.92	2.8	3.79	4.71
0.03	1.74	2.58	3.66	4.53
0.045	1.6	2.39	3.5	4.28
0.06	1.45	2.16	3.2	3.91
0.075	1.2	1.89	2.91	3.64
0.09	1.08	1.73	2.61	3.26
0.105	0.94	1.53	2.34	3.0
0.12	0.86	1.42	2.18	2.8
0.135	0.85	1.42	2.0	2.66
0.15	0.85	1.42	1.99	2.64
0.165	0.85	1.42	1.99	2.64

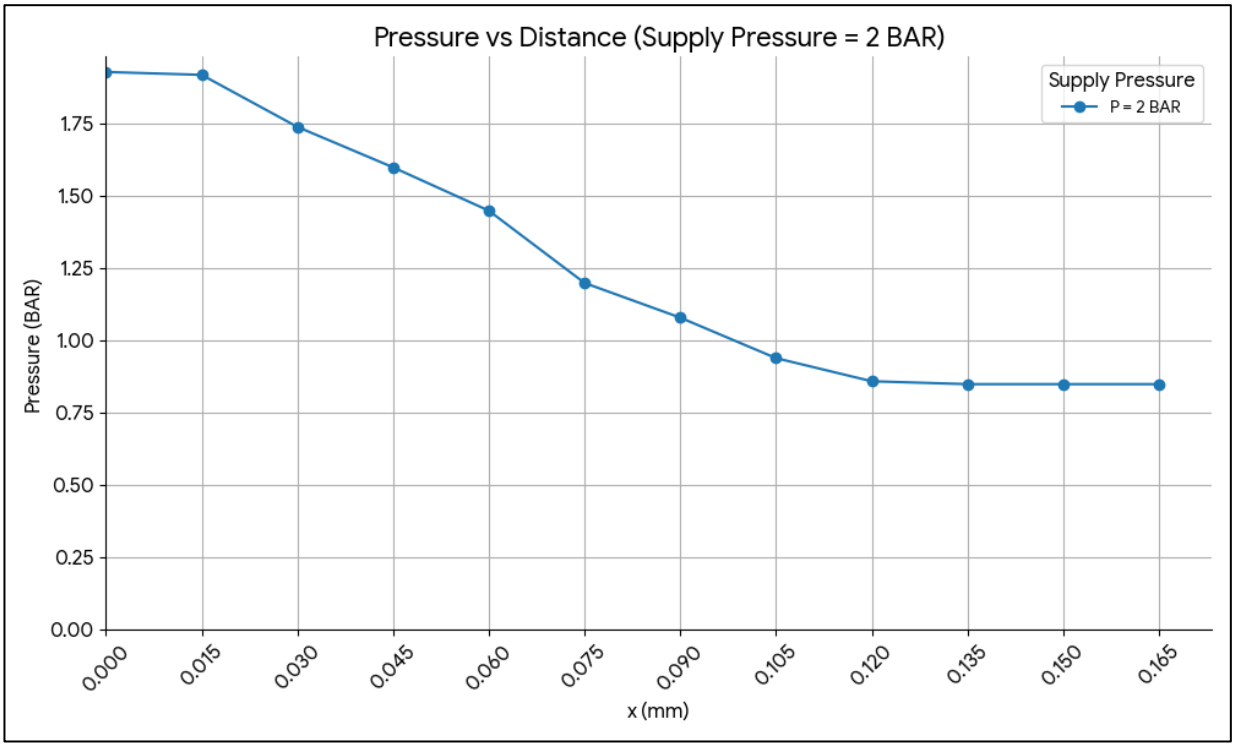

Figure 40:characteristic curve of D1=0.5 D2=0.6 at 2Bar

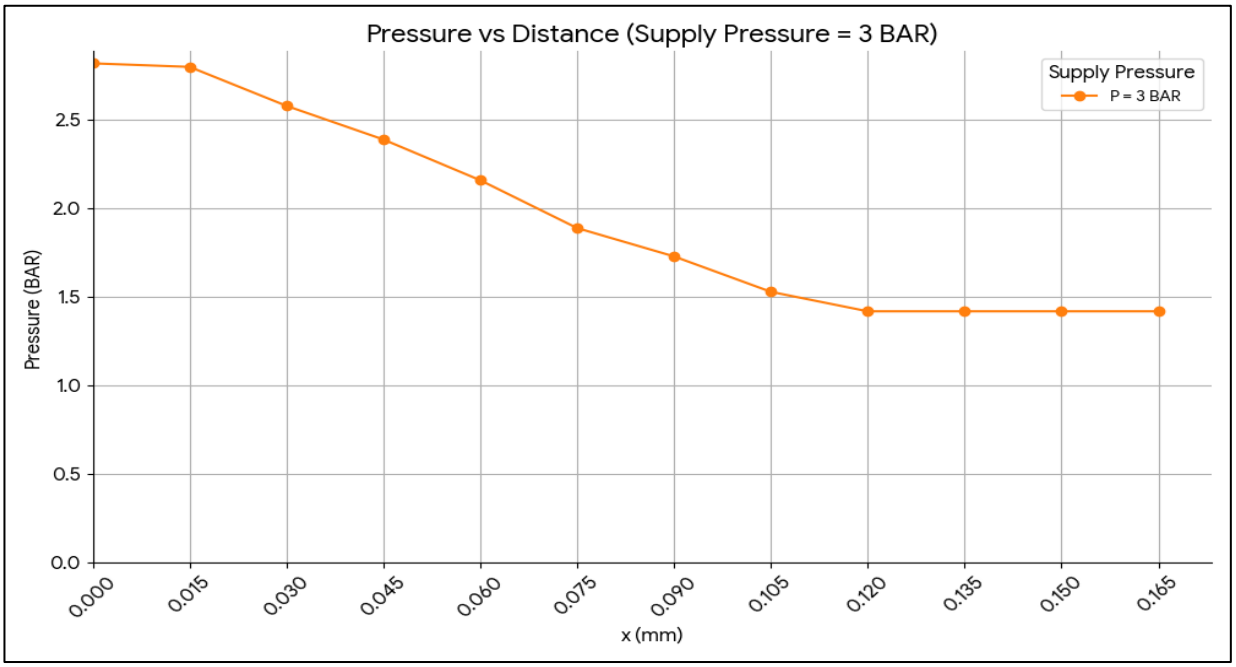

Figure 41: characteristic curve of D1=0.5 D2=0.6 at 3Bar

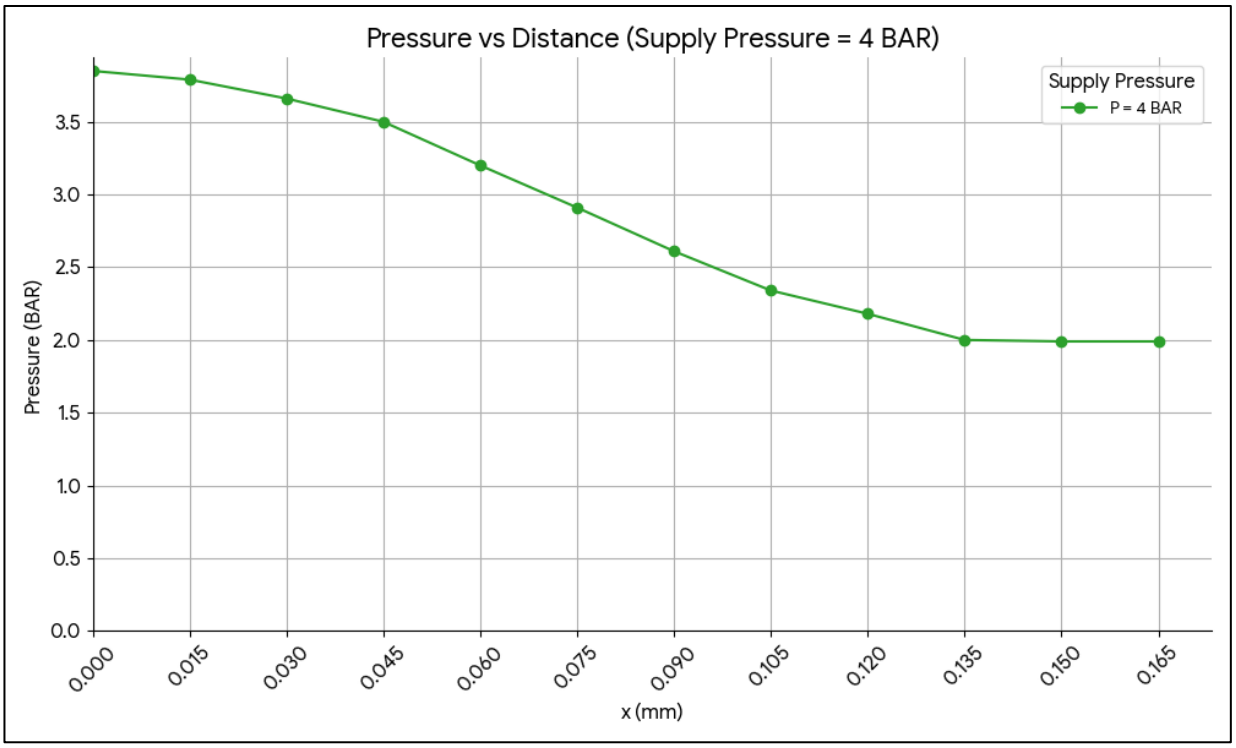

Figure 42: characteristic curve of D1=0.5 D2=0.6 at 4Bar

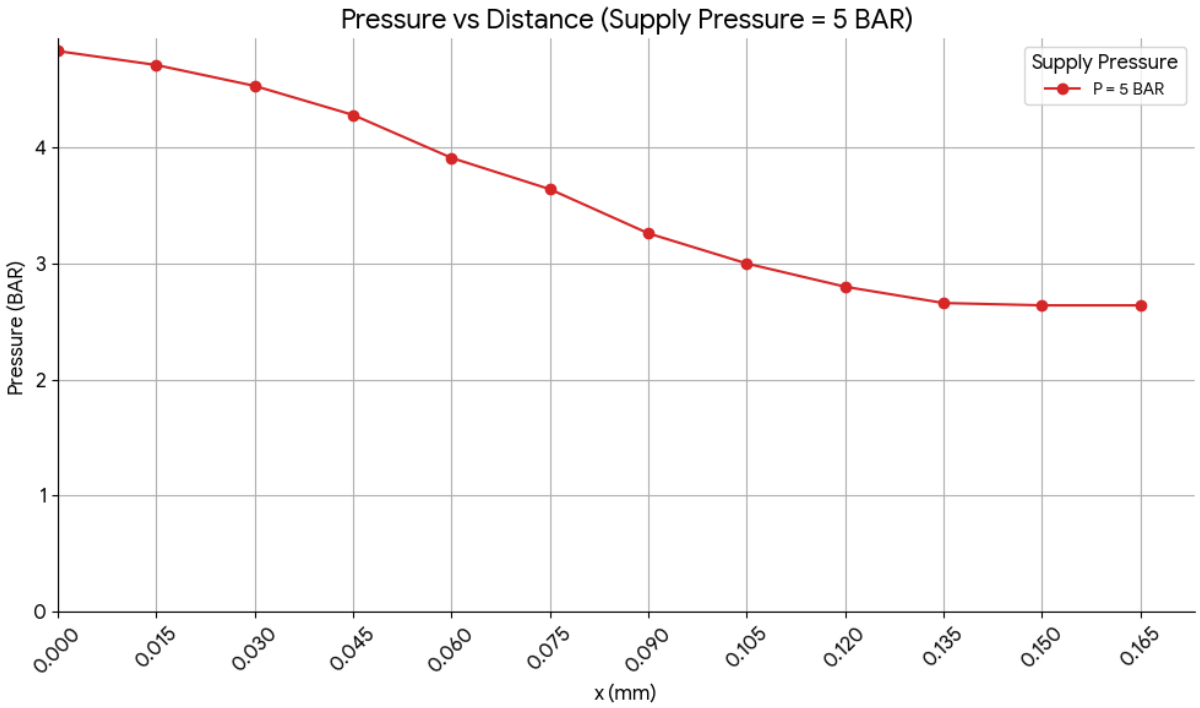

Figure 43: characteristic curve of D1=0.5 D2=0.6 at 5Bar

5.3.2 Experimental Measurements Results of D1 0.4 and D2 0.6

Table 5: Experimental Measurements Results of D1 0.4 and D2 0.6

X(mm)	2(BAR)	3(BAR)	4(BAR)	5(BAR)
0	1.99	3.00	3.92	4.96
0.015	1.97	2.94	3.87	4.95
0.03	1.84	2.87	3.87	4.92
0.045	1.81	2.74	3.85	4.89
0.06	1.67	2.57	3.83	4.80
0.075	1.56	2.46	3.75	4.73
0.09	1.41	2.26	3.59	4.57
0.105	1.18	2.11	3.46	4.33
0.12	1.13	1.85	3.22	4.13
0.135	1.05	1.56	3.03	3.79
0.15	0.76	1.32	2.79	3.47
0.165	0.59	1.00	2.36	3.28
0.18	0.48	0.82	2.07	2.67
0.195	0.39	0.73	1.76	2.3
0.21	0.34	0.63	1.41	2.02
0.225	0.3	0.63	1.24	1.67
0.24	0.28	0.63	1.02	1.51
0.255	0.28	0.63	0.97	1.36

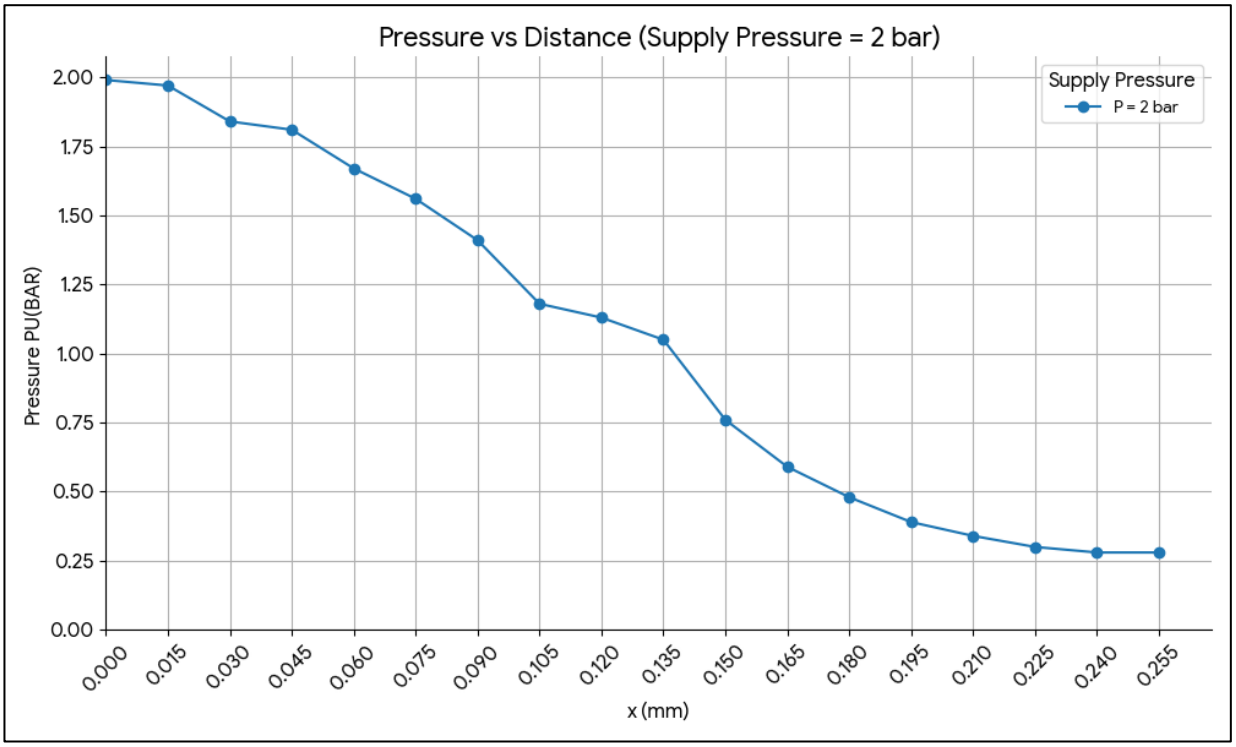

Figure 44: characteristic curve of D1=0.4 D2=0.6 at 2Bar

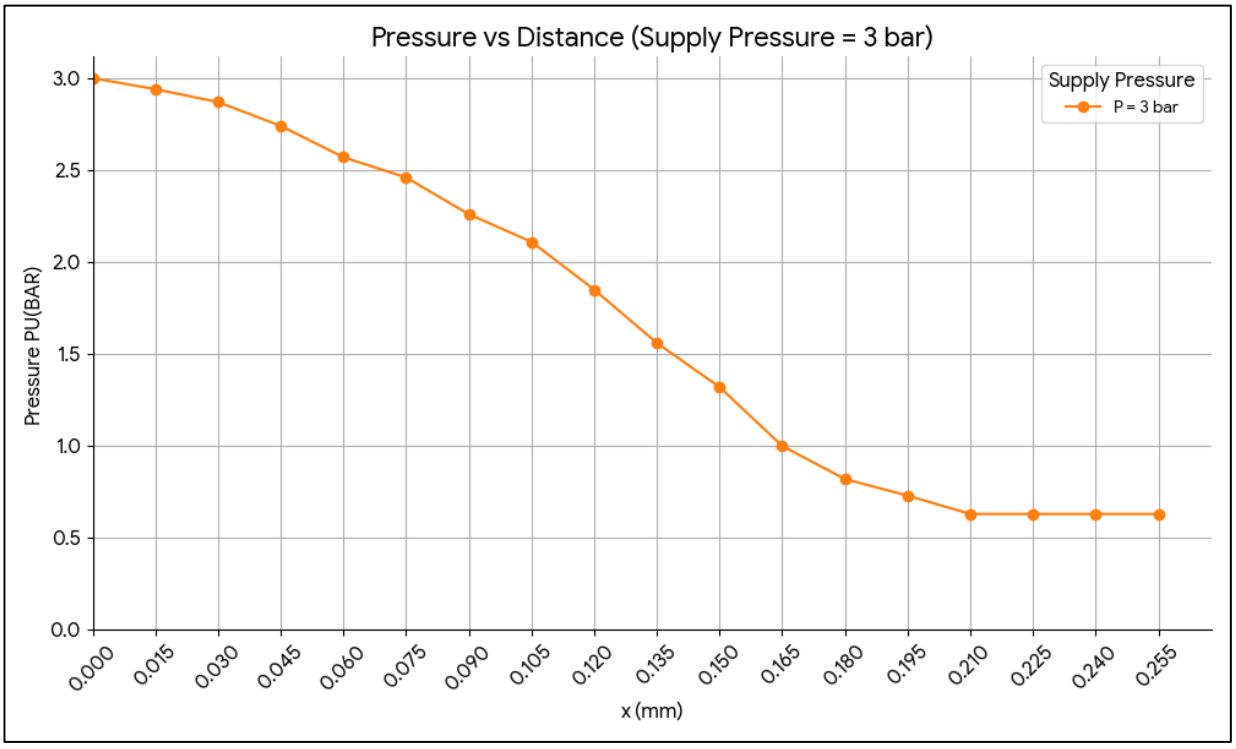

Figure 45: characteristic curve of D1=0.4 D2=0.6 at 3Bar

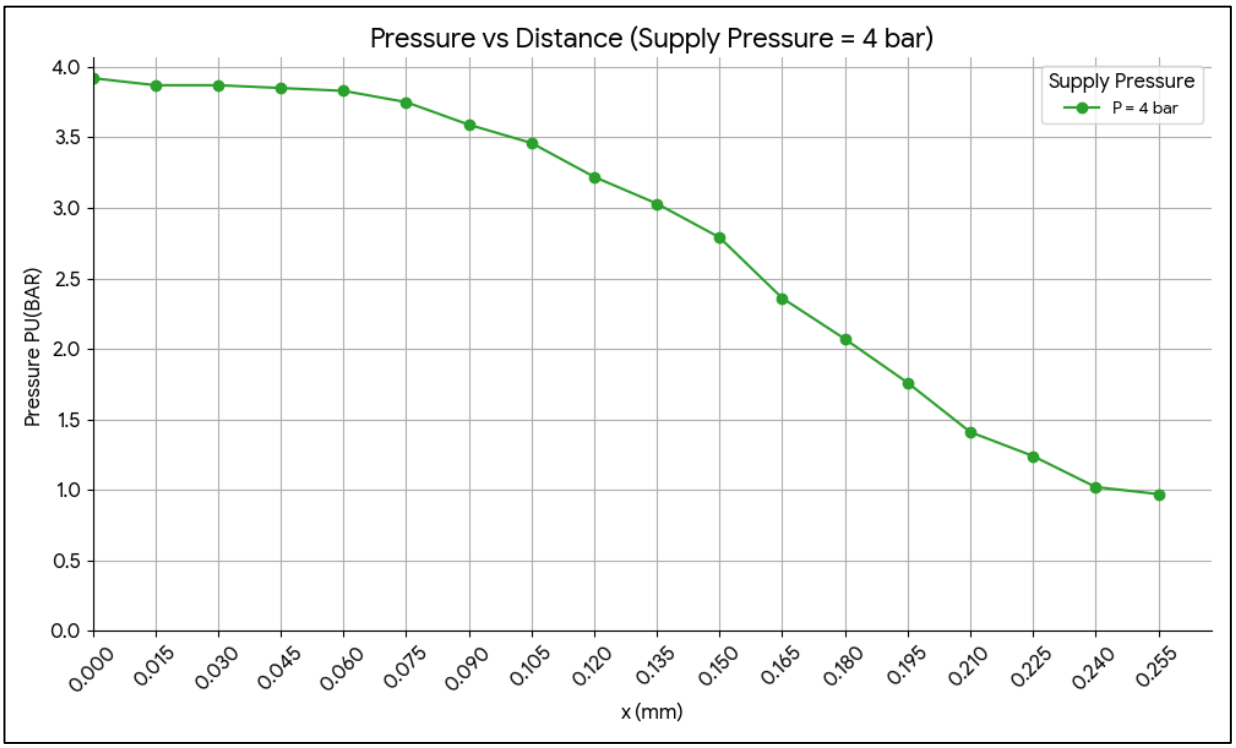

Figure 46: characteristic curve of D1=0.4 D2=0.6 at 4Bar

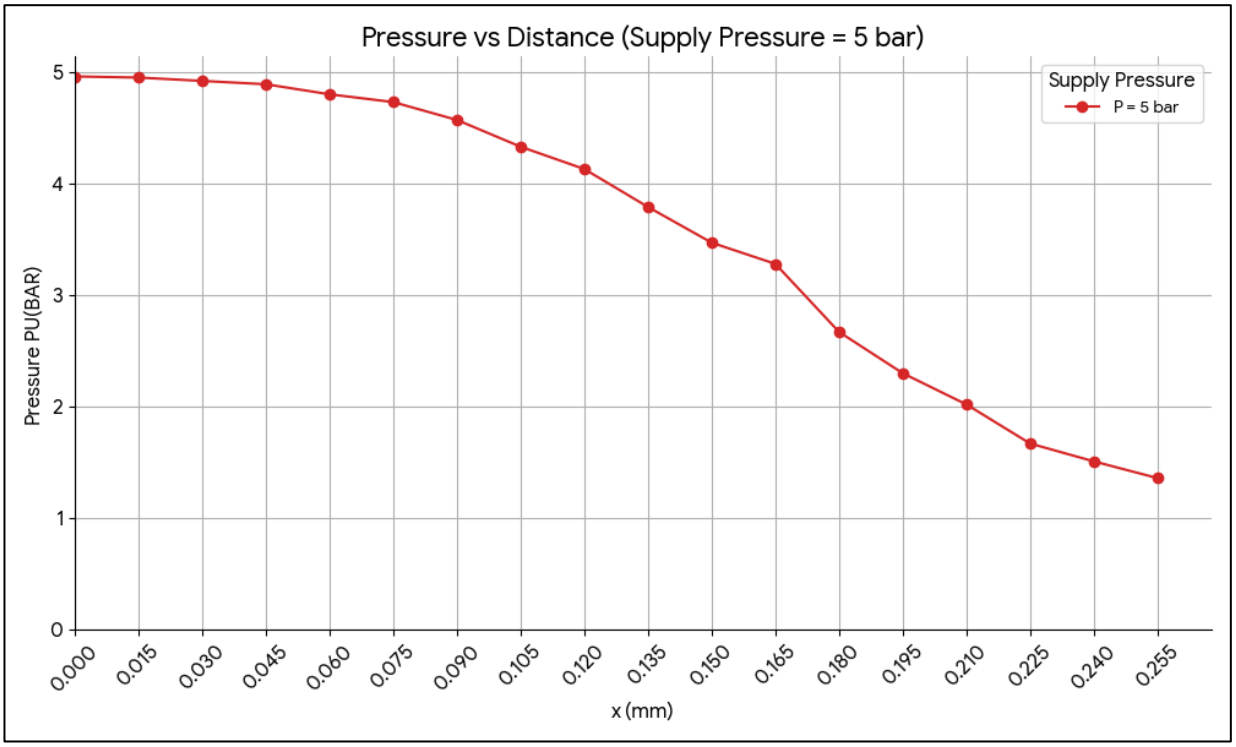

Figure 47: characteristic curve of D1=0.4 D2=0.6 at 5Bar

5.4 Hysterias Analysis:

During the experimental testing phase, the sensor was subjected to both increasing and decreasing pressure cycles. This method was implemented to assess the sensor's dynamic response and evaluate its ability to accurately capture pressure changes in both directions. Monitoring the sensor output under these varying conditions is essential for determining its consistency, reliability, and overall performance in real-world applications where pressure fluctuations are common.

5.4.1 Graph Plotting

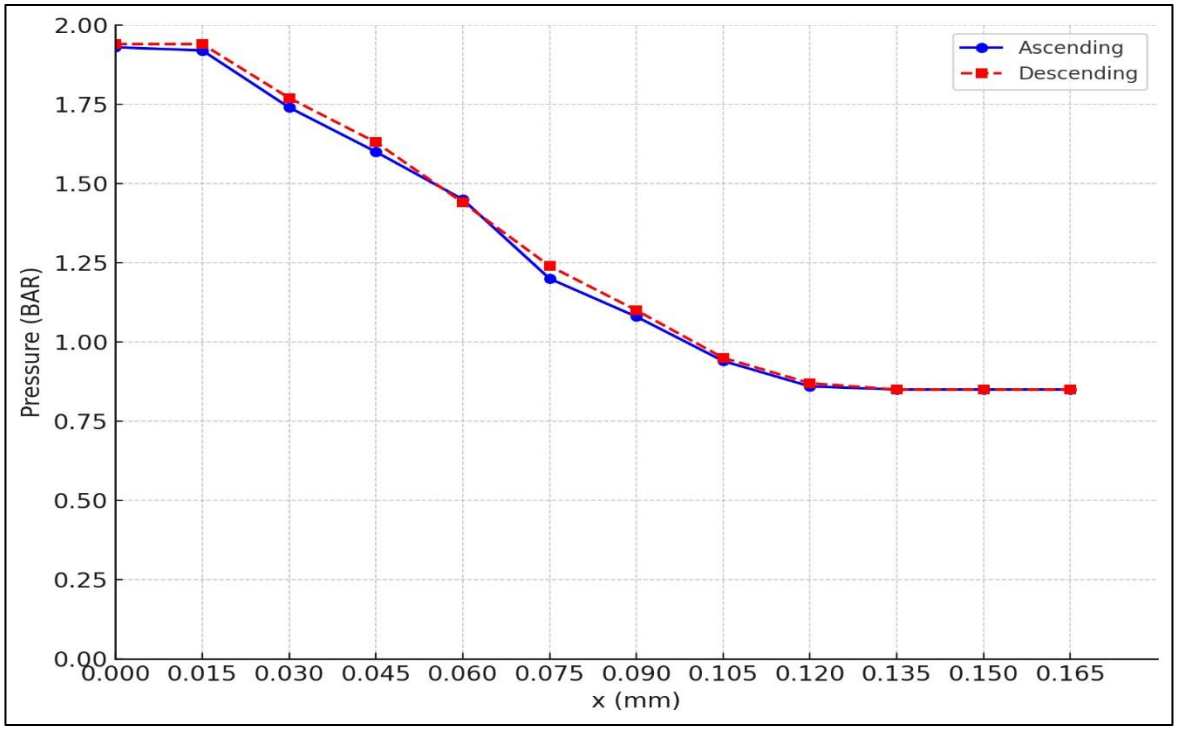

Figure 48: Sensor Response at 2 BAR: Ascending vs Descending Displacement

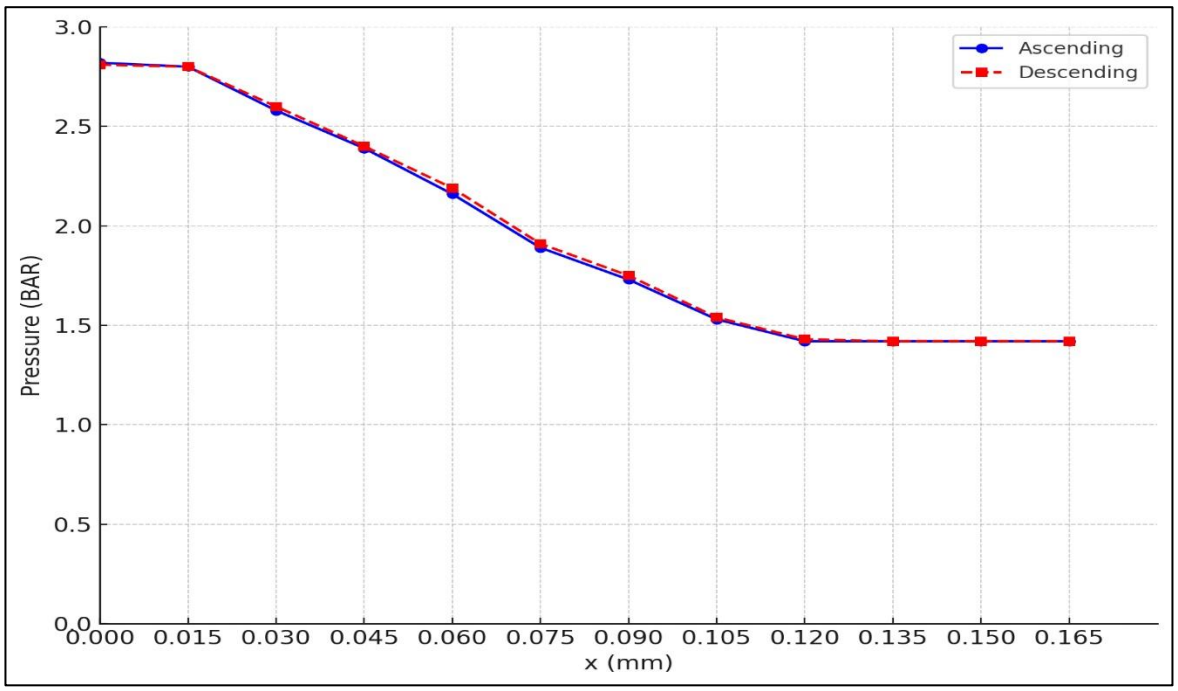

Figure 49: Sensor Response at 3 BAR: Ascending vs Descending Displacement

5.4.2 Hysterias Analysis:

Following the data acquisition, a comparative analysis was performed between the readings obtained during the upward and downward pressure cycles. This analysis aimed to identify any discrepancies that could indicate hysteresis, offset, or other performance-related deviations. A strong correlation between the two datasets would confirm the sensor's stability and accuracy, whereas notable differences would highlight the need for further design refinement.

5.5 Comparison Between CFD Simulations and Experimental Results

To assess the reliability of the computational model, numerical results obtained from Computational Fluid Dynamics (CFD) simulations were systematically compared with experimental data. The comparison examines the pressure response of the sensor as a function of

displacement under varying applied pressure levels. This analysis aims to evaluate the predictive capability of the CFD model and to validate its agreement with the physical behavior observed in the experimental measurements.

5.5.1 Characteristic Curves comparison for D1=0.4 and D2=0.6

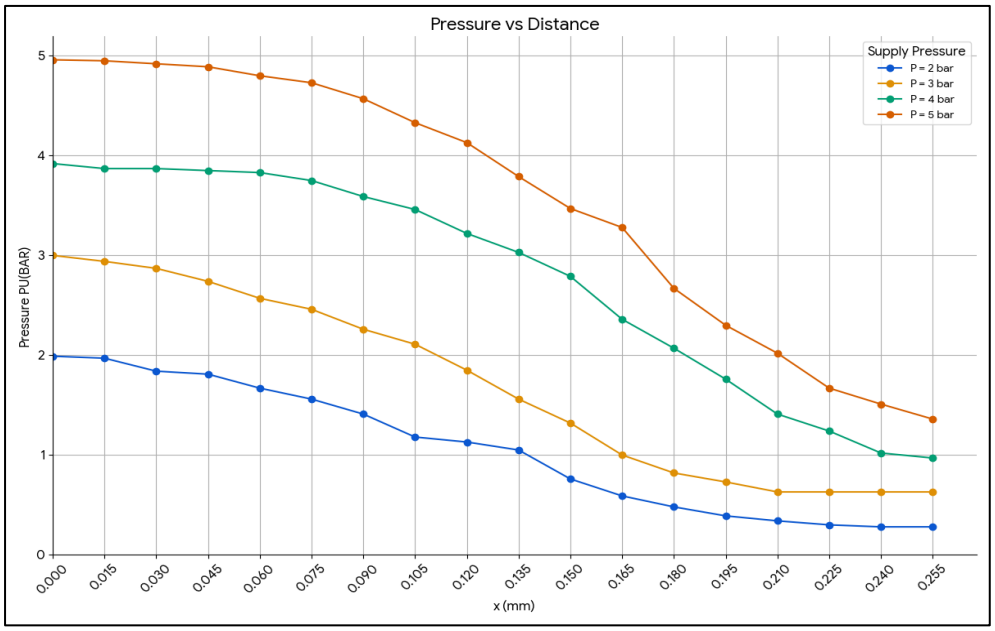

Figure 50: characteristic curves of D1=0.4 D2=0.6 at 2,3,4,5 Bar- Experimental

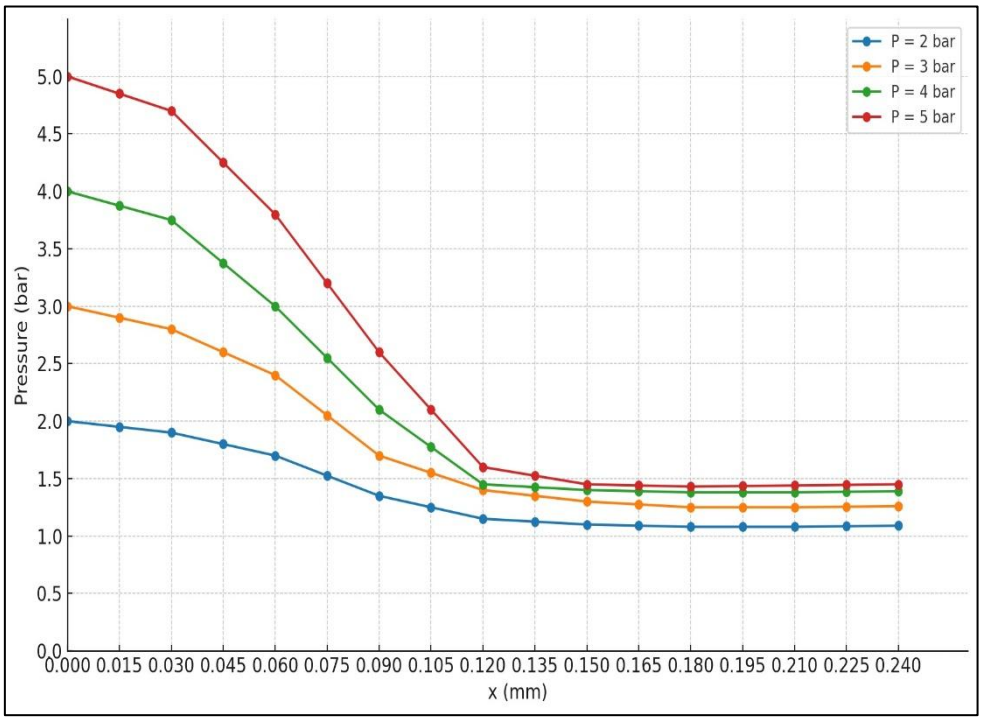

Figure 51: characteristic curves of D1=0.4 D2=0.6 at 2,3,4,5 Bar- CFD

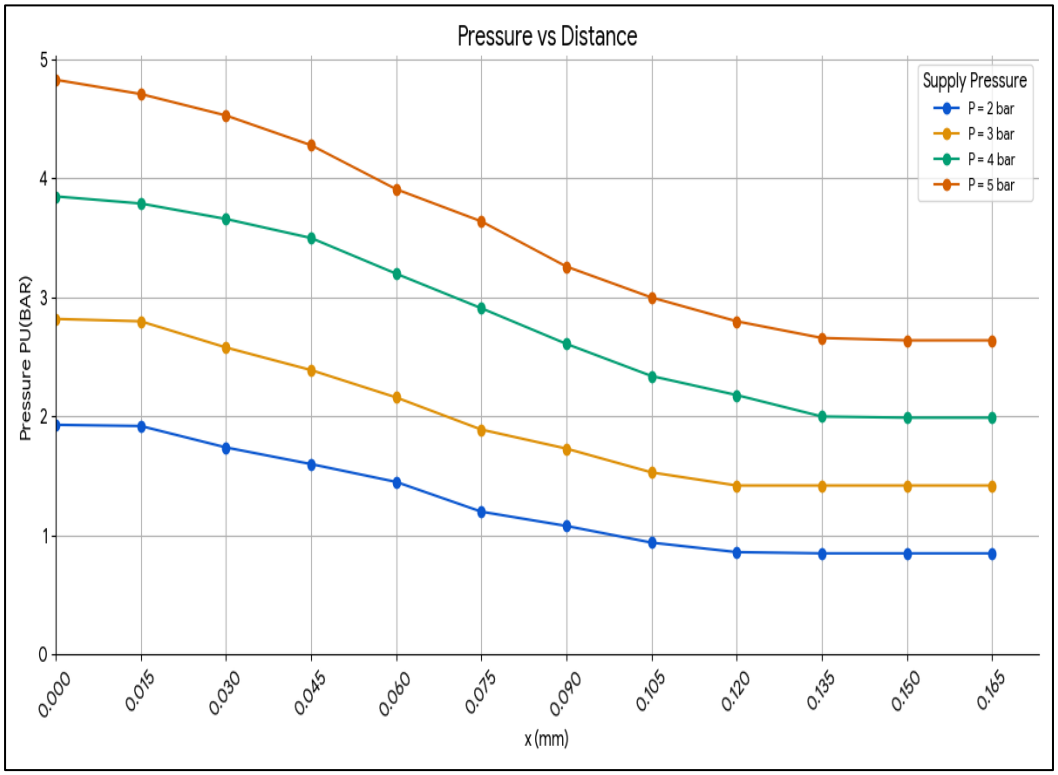

Figure 52: characteristic curves of D1=0.5 D2=0.6 at 2,3,4,5 Bar- Experimental

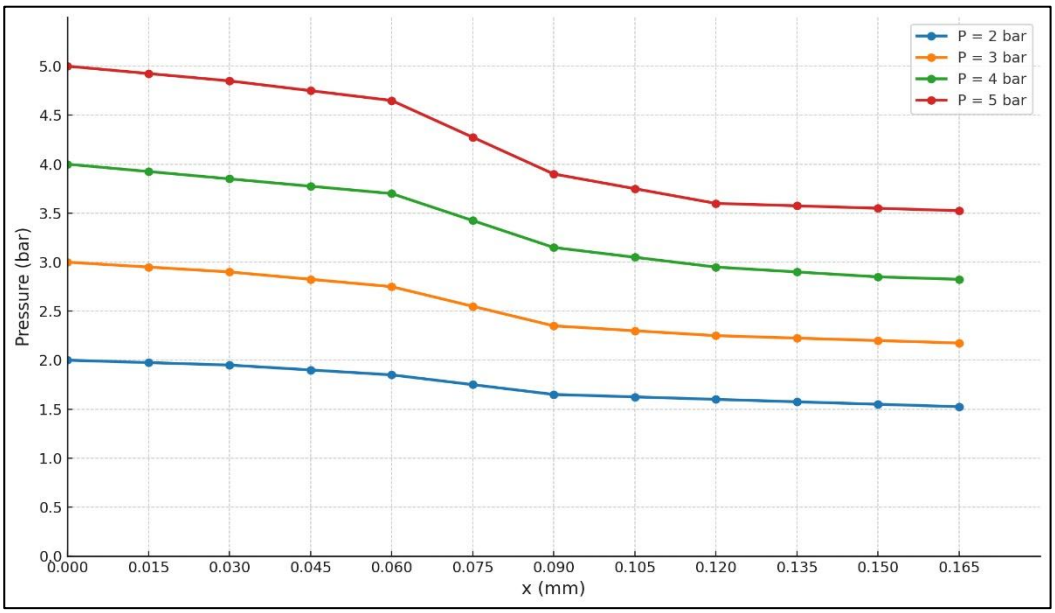

Figure 53: characteristic curves of D1=0.5 D2=0.6 at 2,3,4,5 Bar- CFD

5.6 Conclusion on Design Comparison

The simulation results for the two-nozzle design 1 (D1 = 0.4 mm, D2 = 0.6 mm) and design 2 (D1 = 0.5 mm, D2 = 0.6 mm) in both CFD analysis and experimental demonstrate notable differences in pressure behavior as a function of sensor distance (x) for various inlet pressures. In both cases, the PU pressure decreases with increasing distance from the object, eventually stabilizing at a lower value beyond a certain point. However, Design 2 exhibits a more gradual pressure drop and maintains a higher PU pressure over the same distance range compared to Design 1. This indicates that the slightly larger inlet diameter (0.5 mm vs. 0.4 mm) in Design 2 results in a reduced pressure loss and more consistent pressure readings, especially at higher inlet pressures (4–5 bar). Moreover, the characteristic curves for Design 2 are smoother and exhibit fewer steep gradients, suggesting improved flow stability. In contrast, Design 1 shows a sharper pressure decline, particularly at short distances ($x < 0.15$ mm), implying higher sensitivity to position but potentially less robustness in real-world applications. Therefore, from both a performance and stability perspective, the configuration with D1 = 0.5 mm and D2 = 0.6 mm is more favorable for applications requiring consistent and reliable pressure sensing across a range of distances.

References:

Adafruit. (2023). *Infrared sensors: A guide*. Retrieved from https://www.adafruit.com

Baumer. (n.d.). Precise laser sensor for detection of very small objects to 0.05 mm [Product page]. Retrieved July 5, 2025, from https://www.baumer.com/us/en/precise-laser-sensor-for-detection-of-very-small-objects-to-0-05-mm/n/O200-miniature-sensors-reliable-precise-simple-and-digital

Belforte, G., Manuello Bertetto, A., & Raparelli, T. (1995, June 12–16). Back pressure sensor for very high precision measurement. In *Proceedings of the Fourth International Symposium of Measurement and Control in Robotics* (pp. 63–70). Smolenice Castle, Slovakia.

Belforte, G., Mazza, L., & Visconte, C. (2012). Non-contact wear measurement on pneumatic seals. *Tribology International, 48*, 73–77. https://doi.org/10.1016/j.triboint.2011.11.004

Circuits-Elec. (n.d.). *Infrared proximity sensor 5–36V* [Product page]. Retrieved August 3, 2025, from https://circuits-elec.com/products/infrared-proximity-sensor5-v-36-v?srsltid=AfmBOoqRp01bPbJ7ptReuu7FNkGWdFyMsxOSY945Sjd0obryWDcSzUSR

Honeywell. (2022). *Environmental factors in ultrasonic sensors*. Retrieved August 3, 2025, from https://sensing.honeywell.com/environmental-factors-ultrasonic-sensors

Jacobs, B. E. A. (1972). *Fluidic sensors and some large-scale devices*. Springer-Verlag Wien-New York.

Leica. (2022). *Precision laser sensors*. Retrieved from https://www.leica-geosystems.com

Manuello Bertetto, A., & Mazza, L. (1996, June 4–6). A very high precision system to measure wear in elastomeric seals. *IEEE Instrumentation and Measurement Technology Conference*, Brussels, Belgium.

Mech Poriyaan. (n.d.). *Fluid sensors*. Retrieved from https://mech.poriyaan.in/topic/fluid-sensors-31626/

Mech Poriyaan. (n.d.). *Review and summary of fluid sensors*. Retrieved from https://mech.poriyaan.in/topic/review-and-summary-31634/

Mofidi, M., & Prakash, B. (2008). Influence of counterface topography on sliding friction and wear of some elastomers under dry sliding conditions. *Proceedings of the Institution of Mechanical Engineers, Part J: Journal of Engineering Tribology, 222*(J4), 667–673.

Omron. (2021). *Capacitive sensor applications*. Retrieved August 3, 2025, from https://www.omron.com/sensors/capacitive-applications

Parker Hannifin Corporation. (n.d.). Three-piece radial seal cross-section [Image]. In *Engineered sealing solutions* (p. 20). Parker O-Ring Division. https://www.parker.com/content/dam/Parker-com/Literature/O-Ring-Division-Literature/Engineered-Solutions-20---Three-Piece-Seal.pdf

Pepperl+Fuchs. (2018). [Ultrasonic sensor detection range diagram] [Image]. In *Ultrasonic sensor FAQ: Detection range and accuracy*. https://blog.pepperl-fuchs.com/en/2018/ultrasonic-sensor-faq-detection-range-and-accuracy/

Poriyaan.mech. (n.d.). Cone-jet proximity sensor diagram [Image]. *Fluid sensors educational materials*. https://mech.poriyaan.in/

Poriyaan.mech. (n.d.). Figure 15.11: Cone-jet proximity sensor [Diagram]. In *Fluid sensors*. https://mech.poriyaan.in/topic/fluid-sensors-31626/

Poriyaan.mech. (n.d.). Figure 15.12: Interruptible jet sensor [Diagram]. In *Fluid sensors*. https://mech.poriyaan.in/topic/fluid-sensors-31626/

RealPars. (2024). Sensor adjustment screw. In *Capacitive sensors explained*. https://www.realpars.com/blog/capacitive-sensor

RealPars. (2024). Inductive-sensor-sensing-range.jpeg [Photograph]. In *Inductive proximity sensors: The complete guide*. https://www.realpars.com/blog/inductive-sensor

Schneider Electric. (2023). *Inductive proximity sensors*.

SensComp. (2021). *Ultrasonic sensors overview*. Retrieved August 3, 2025, from https://www.senscomp.com/ultrasonic-sensors-overview

Sharp Electronics. (2023). *Infrared sensor applications*. Retrieved August 3, 2025, from https://www.sharpsma.com/infrared-sensors-applications

SICK. (2023). *Laser distance measurement*. Retrieved August 3, 2025, from https://www.sick.com/products/laser-distance-measurement

Stockwell Elastomerics. (2020, May 22). Seal, notched [Photograph]. *Stockwell Elastomerics*. https://www.stockwell.com/blog/static-seal-failure-modes/